Sulfuric Acid Dispersion and Injection Engine (SADIE-65)

Final Report

by

Team Skunk-Don’t-Works

Group 01

Gabriel Carey

Xuan Nie

April. 10, 2024

Contents

List of Figures

List of Tables

Executive Summary

The Sulfuric Acid Dipersion and Injection Engine, or SADIE-65, is a conceptual aircraft designed by Team Skunk-Don't-Works for the AIAA 2023-24 design competition, as part of a project for AERO3002 at Carleton University, under the instruction of Dr. Ed. Cyr. The purpose of this document is to outline the development of the conceptual design for this new aircraft.

The main goal behind the project is to design an aircraft capable of flying at high altitudes to disperse a liquid payload into the atmosphere, as a means of solar radiation management (SRM) to reduce global temperatures. The aircraft must also meet a predetermined set of performance requirements provided in the AIAA RFP., and be certified to FAA 14 CFR Part 25.

The final design for SADIE exceeds the performance requirements, and meets all certifications under 14 CFR Part 25. The selling price is $40 million USD with a 33% markup, with direct operating costs falling just under $10 million for each aircraft. In order to meet the desired annual payload dispersion requirements, a fleet size of 300 will be in service after the first 10-year production period. The proposed solution will permit stratospheric payload delivery of aerosolized sulfuric acid, in an attempt to cool the planet down to acceptable temperatures as a short-term solution to the global climate crisis. Further development of the concept will allow for improved cost reductions and fuel efficiency, reducing the amount of emissions and thus aid in the fight against climate-change.

1 CONCEPT SELECTION

1.1 Design Requirements

The primary objective of the Sulfuric Acid Dispersion and Injection Engine, or SADIE, is to provide an aircraft capable of dispersing aerosol particles into the stratosphere. The aim is to diminish solar radiation absorption by the planet and facilitate artificial cooling of global temperatures. According to the requirements outlined in the RFP, the high-altitude aircraft must have the capability to release these particles at an altitude of 65 000 ft [1]. The main requirements are summarized in Table 1-1.

Table 1-1: Summary of main RFP requirements.

Specification	Requirement
Cruise Mach	Greater than or equal to 0.5
Capable of flight in icing conditions	Yes, with de-icing device
Certification	Certified to 14 CFR Part 25
Payload capacity	At least 30 000 lb
Cruise range	400 nm
Ferry range	At least 3000 nm
Time to climb	Less than or equal to 1 hr
Cruise altitude	65 000 ft
VFR and IFR	Capable of both VFR and IFR flight
Maximum takeoff and landing length	Max T-O/LDG field length of 8000 ft over a 50 ft obstacle (@SL, ISA + 61°F)
EIS Date	EIS by 2030

The most notable requirements above are the payload and cruise altitude requirements. A large payload carrying capacity is required, in combination with high altitude flight. As a result, the selected configuration will require a wing design capable of generating ample lift at high altitude, enough to support the moderately heavy weight of the payload along with the inevitably heavy airframe that will result from structural requirements. In addition to the requirements in Table 1-1, a minimum of 3 million metric tons of payload must be dispensed annually. The fleet size for the SADIE project is thus estimated based on this requirement and the predicted yearly flight hours per aircraft. Apart from meeting the above requirements, the main objective is to minimize the cost of designing, building, and operating a single aircraft, per metric ton of payload dispensed on a yearly basis.

1.2 Initial Aircraft Research

Several existing aircraft with similar specifications to the mission requirements are summarized in Table 1-2. Due to the combination of high-altitude flight and a relatively heavy payload, there is currently a lack of existing aircraft capable of handling both requirements simultaneously. Many aircraft can fly at high altitudes, and many aircraft can transport heavy payloads, however few can do both. Historically, aircraft that have been developed and do meet these stringent requirements tend to be military aircraft which fly at supersonic speeds with high operating and production costs, which have not been optimized for the mission at hand. These aircraft are typically designed for reconnaissance purposes, with much design emphases on stealth.

The Boeing B-52 Stratofortress, for example, has great range and payload capacity well exceeding the requirements for the mission. However, the B-52 falls short with a cruise altitude of 50 000 ft. The SR-71 Blackbird was designed as a supersonic reconnaissance aircraft and is capable of flight at an altitude of up to 85 000 ft and can cover a range of over 2000 nm. However, the aircraft only has a payload capacity of 20 000 lb, and flies at speeds far greater than what is necessary for the mission, only lending itself to increased operational and production costs and a more complex design. Similar to the SR-71, the XB-70 meets the cruise range and altitude requirements, however the high supersonic speeds and low payload capacity render it ineffective in completing such a mission. The U2 Dragon Lady is a reconnaissance aircraft with a service ceiling of 80 000 ft, commonly flown at altitudes above 70 000 ft, exceeding the cruise altitude requirement for the mission. Despite having a high service ceiling, the U2 only has a payload capacity of about 5 000 lb, six times less than what is required, with a gross weight which is only 4/3 the needed payload capacity. Despite some aircraft meeting a few of the mission requirements, no aircraft currently exists which is well optimized for this mission.

Table 1-2: Existing aircraft with similar mission capabilities.

Name	Spec	Value	Comments
B-52 Stratofortress [2]	Gross Weight	195 000 lb	Within the design range; slightly heavy for the required payload
	Cruise Speed	510 mph (M 0.772)	Meets the requirement
	Cruise Altitude	50 000 ft	Slightly less than requirement
	Range	6 380 nm 8 685 nm (F)	Far exceeds the requirement of the mission
	Cost	$101 million (Estimated)	The cost is relatively high for the mission
	Payload	70 000 lb	More than double of the requirement
	Thrust	136 000 lb	Slightly more thrust than required

SR-71 Blackbird [3]	Gross Weight	60 000 lb	Fairly low; good for design, may increase cost
	Cruise Speed	2 275 mph (M 3.35)	Far too high for the mission; supersonic speed results in increased costs
	Cruise Altitude	80 000 ft	Exceeds the design requirement of 65 000 ft
	Range	2 590 nm (F)	Slightly less than the requirement
	Cost	$322 million	Too high for this mission
	Payload	20 000 lb	Does not meet the requirement
	Thrust	65 000 lb	TWR greater than 1, too large for mission
XB-70 Valkyrie [4]	Gross Weight	300 000 lb	Too heavy; too much thrust required to carry payload
	Cruise Speed	2 056 mph (M 3.11)	Far too high for the mission; supersonic flight results in dramatic increase of costs
	Cruise Altitude	73 000 ft	Exceeds design requirement
	Range	6 600 nm	Far greater than requirement
	Cost	$700 million (Estimated)	Far too high for the mission
	Payload	20 000 lb	Does not meet the requirement
	Thrust	180 000 lb	TWR greater than what is required
U2 Dragon Lady [5]	Gross Weight	40 000 lb	Too low to carry the payload
	Cruise Speed	410 mph	Slightly below the requirement
	Cruise Altitude	70 000 ft	Meets the requirement
	Range	6 090 nm	Exceeds the mission requirement
	Payload	5 000 lb	Does not meet the requirement
	Thrust	17 000 lb	TWR greater than what is required

The aircraft specs from above are calculated in terms of dimensionless fractions of the mission requirement for that specification and plotted in Figure 1-1. Values greater than 1 indicate that the requirement is met, less than 1 the requirement is not met. The SR-71 and XB-70 meet all

requirements except for payload capacity. Although these aircraft appear to fit the requirements well, they are highly suboptimal for this particular mission. They are supersonic aircraft which cost hundreds of millions of dollars to acquire and operate, and are primarily designed for reconnaissance, not payload-dispersion. Thus, only the B-52 and U2 will be compared. Both aircraft meet the cruise speed requirement, however the B-52 falls short of cruise altitude, and the U2 falls short of payload capacity. Three-view drawings for both the B-52 and U2 are provided in Figure 1-2 and Figure 1-3, respectively.

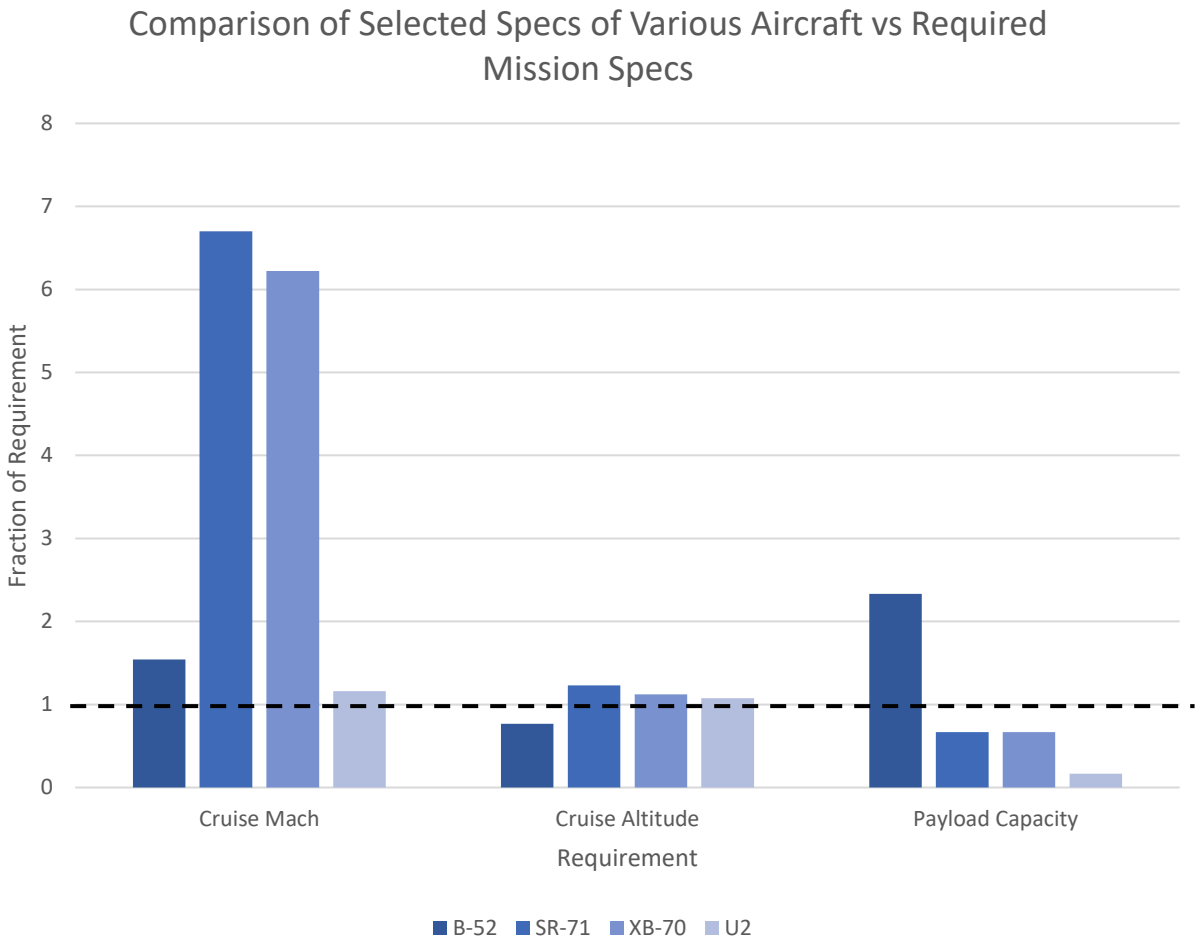

Figure 1-1: Comparison of various aircraft specs to mission requirements.

By comparing the planforms of both aircraft, some similarities can be observed. Most notably is the high aspect ratio on both designs, characteristic of high-altitude aircraft. High aspect ratios tend to have higher span efficiencies, as they reduce the amount of wingtip vortices which reduce the lift of the wing. Thus, high aspect ratio wings fare better in high altitude flight where

the air is much thinner, where less thrust is produced. The B-52 is much larger, with a wing area nearly four times greater than the U2, to account for the much heavier weight. It stands to reason that the initial design for SADIE will be similar to that of the B-52 and the U2, with a lighter MTOW than the B-52, and a greater wing area than the U2. This should allow for a compromise between the high payload capacity of the B-52 and the high altitude of the U2.

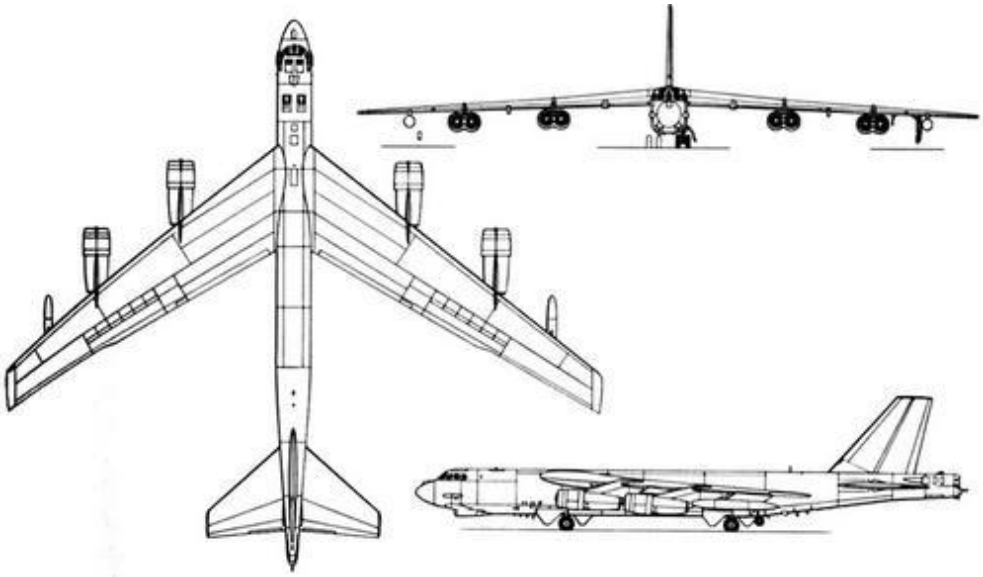

Figure 1-2: Three-view drawing of B-52 “Stratofortress” [6].

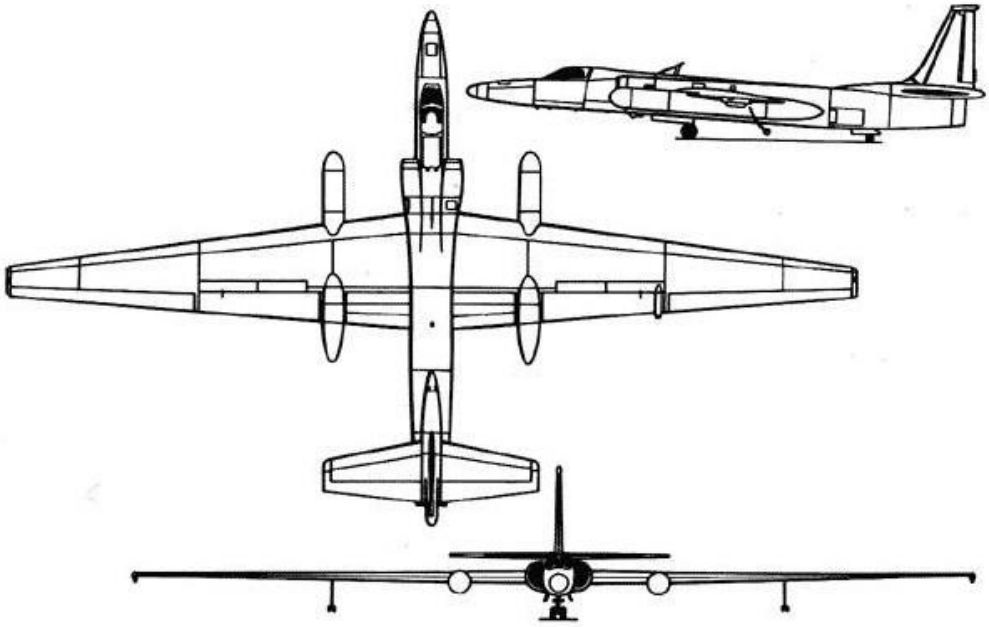

Figure 1-3: Three-view drawing of U2 “Dragon Lady” [7].

1.3 Concept Sketches

The first concept sketch for SADIE-65 is presented in Figure 1-4. This initial configuration is reminiscent of a typical business jet, which served as inspiration for several of the initial designs as they are capable of flying at high altitudes upwards of 50 000 ft. The design features dual aft-mounted low-bypass turbofans on the fuselage. The wings are mounted to the bottom of the fuselage to permit sufficient space along the interior for the payload tank. The wings themselves have moderate sweep to increase the critical Mach number, allowing the plane to fly at higher speeds before the formation of shockwaves along the wing. A small dihedral angle improves roll stability for the low-mounted wings. A fairly high aspect ratio improves the aerodynamic efficiency with the wing, as well as the winglets which reduce the presence of wingtip vortices, thus further reducing the drag. The cruciform tail improves the location of the CG.

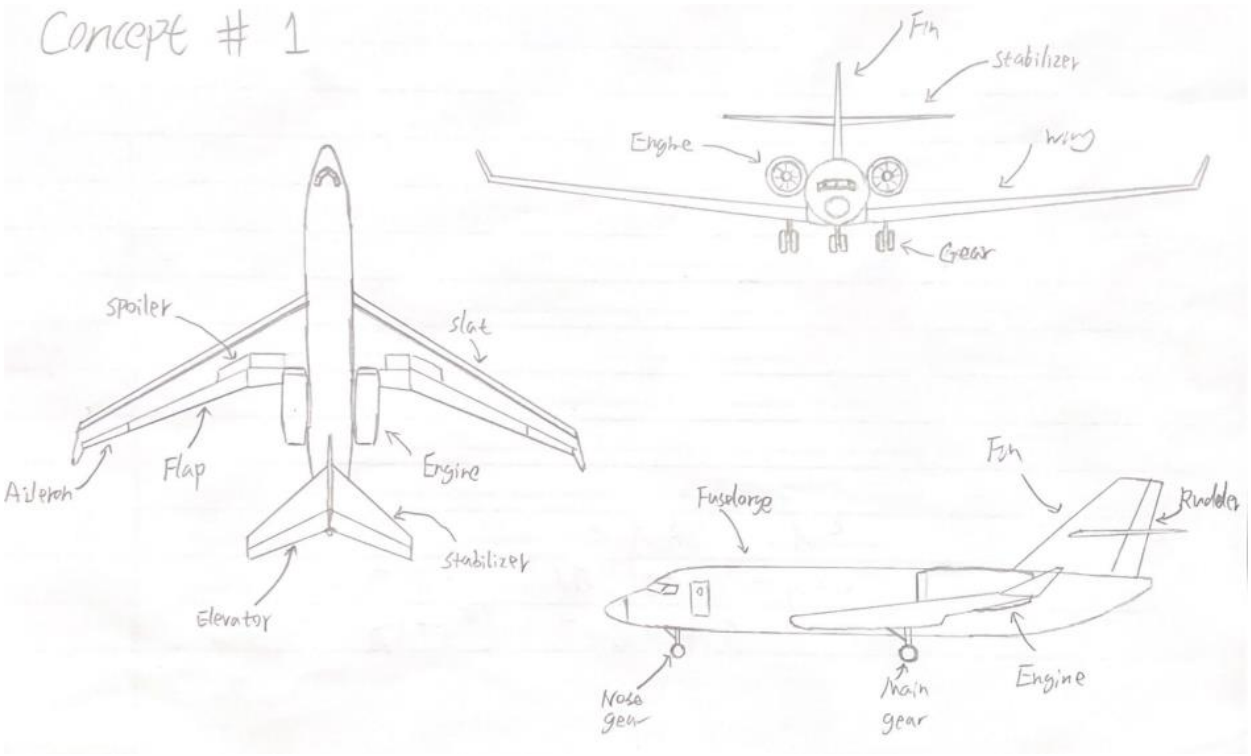

Figure 1-4: Concept sketch of configuration 1.

One primary concern with the above concept was the location of the CG and the size of the aircraft, as the large payload would constitute a significant portion of the gross weight of the aircraft and depending on the location of the payload tank within the fuselage, the CG could be located too far aft due to the location of the engines. Existing trends also show that most business jets, which the concept is based off of, fall short of the required payload capacity, thus

the wings would need to be scaled to achieve the required lift to meet the large payload requirement. This leads to the development of the second concept in Figure 1-5. Several changes are made to the geometry of the aircraft. Firstly, the fuselage is scaled up slightly, along with the low-mounted wings. The aspect ratio from the first concept was maintained, and the wingtips removed. The number of engines was doubled and moved below the wing, to both account for the increased thrust requirement from the greater weight and to shift the CG forward. The tail configuration was switched to a conventional tail, as the cruciform tail was no longer required with the above changes. The biggest changes include the increase in wing area and total thrust to accommodate the larger weight. All other wing parameters are maintained, such as the aspect ratio, dihedral, control surfaces, etc. This design also closely resembles that of a modern-day jet airliner.

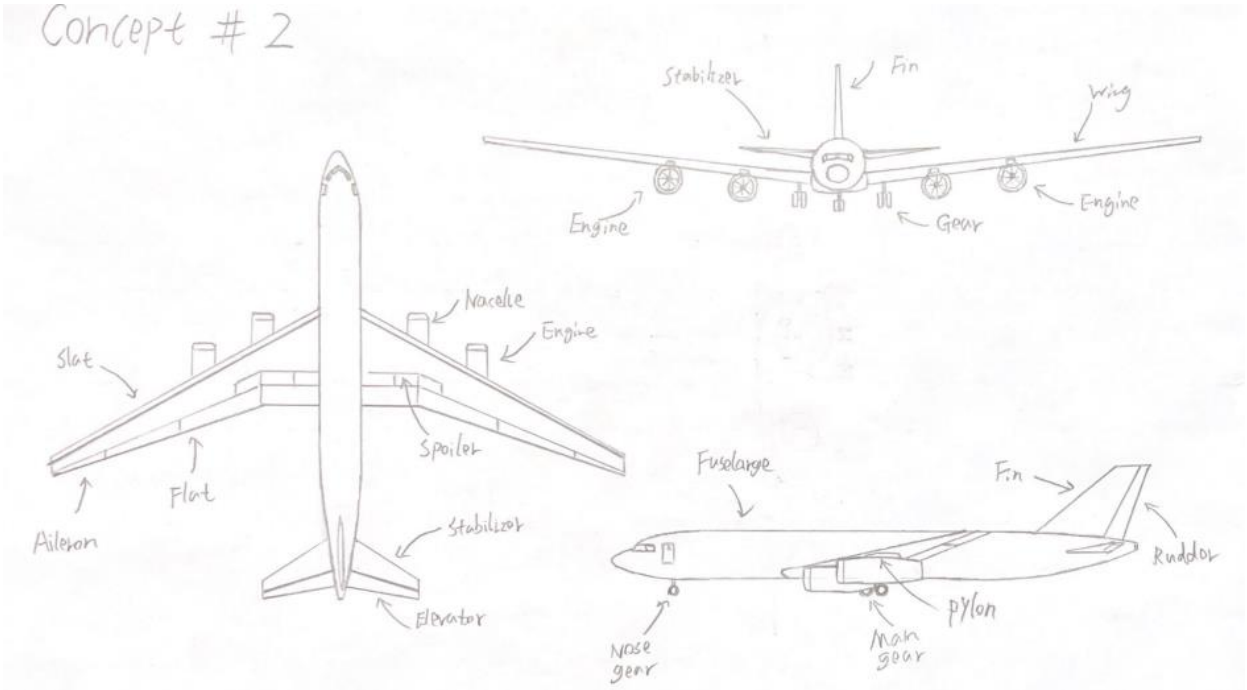

Figure 1-5: Concept sketch of configuration 2.

The third concept is shown in Figure 1-6. Only two adaptations were made from the second concept: the raising of the wing to the top of the fuselage and the removal of the wing dihedral, to switch to a shoulder-mounted flat wing configuration. All other design parameters were unchanged. The main reason for the change was to increase the clearance between the wing and the ground, to accommodate larger engines during takeoff and landing. The increased clearance also allows for ease of inspection and maintenance of the fuselage, as well as any potential fueling or loading/unloading of the payload. The added roll stability from the shoulder-mounted wing also eliminates the need for wing dihedral, thus fair maneuverability can be

maintained with a flat wing. One additional minor benefit from this modification is that the configuration is similar to that of other transport aircraft, so the plane now more resembles other aircraft from the same class, as opposed to looking like a typical jet airliner which would provide a misleading interpretation for the purpose of the aircraft,

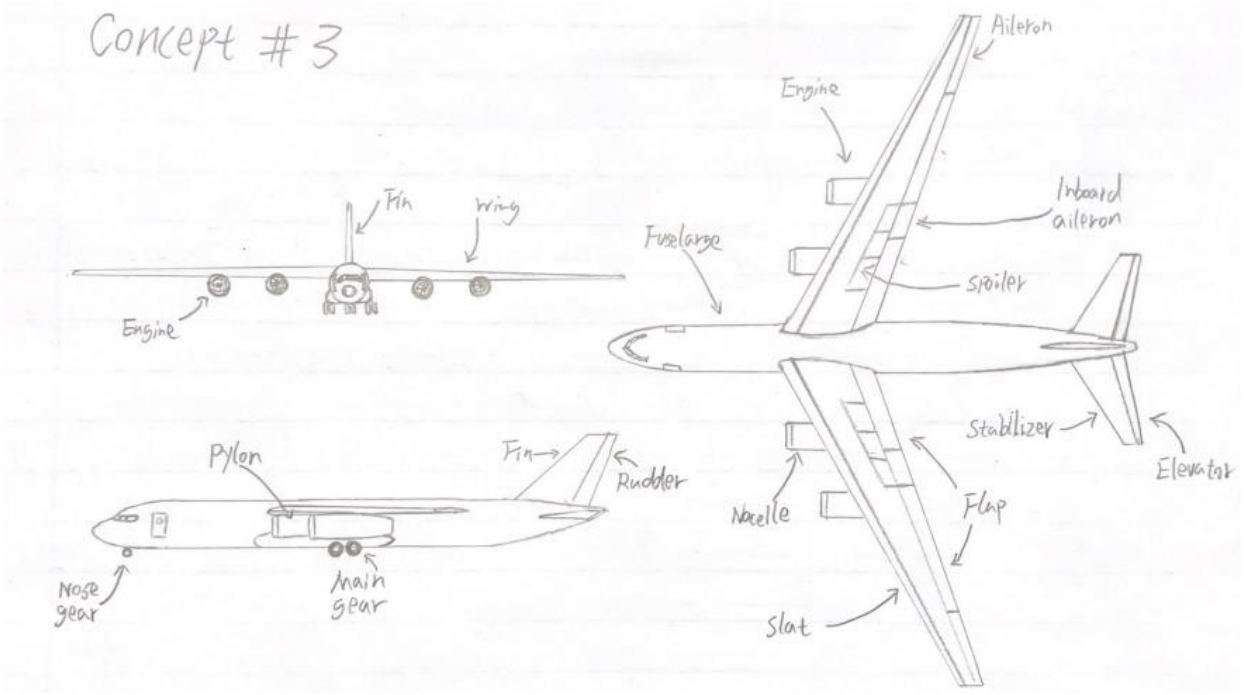

Figure 1-6: Concept sketch of configuration 3.

A rough sketch of the internal layout for the third configuration is provided in Figure 1-7. The pressurized cockpit is located at the fore of the fuselage, with enough space and seating to accommodate the designated four crew members. A weather radar is housed at the nose of the aircraft, enclosed by the radome. The avionics bay is located at the rear of the cockpit. Moving further aft into the cargo bay a cylindrical tank constructed of high-density polyethylene (HDPE) is used to store the 30 000 lb of sulfuric acid. The use of HDPE reduces the overall gross weight of the aircraft and is rated for safe storage of strong sulfuric acid. The tank can be filled from inside the fuselage. A system of pipes and valves lead to a specialized nozzle external to the fuselage, which is used to aerosolize the liquid sulfuric acid payload into the atmosphere. The payload is gravity-fed through a globe-valve, which is necessary to regulate the flow rate to ensure it stays constant for the duration of the flight. The nozzle is designed such that it is located far enough away from the fuselage, such that the dispersed particles do not come into contact with the bottom of the fuselage and corrode the surface. Payload dispersion may be

completely automated or controlled remotely from the cockpit. The auxiliary power unit (APU) is located at the rear of the fuselage.

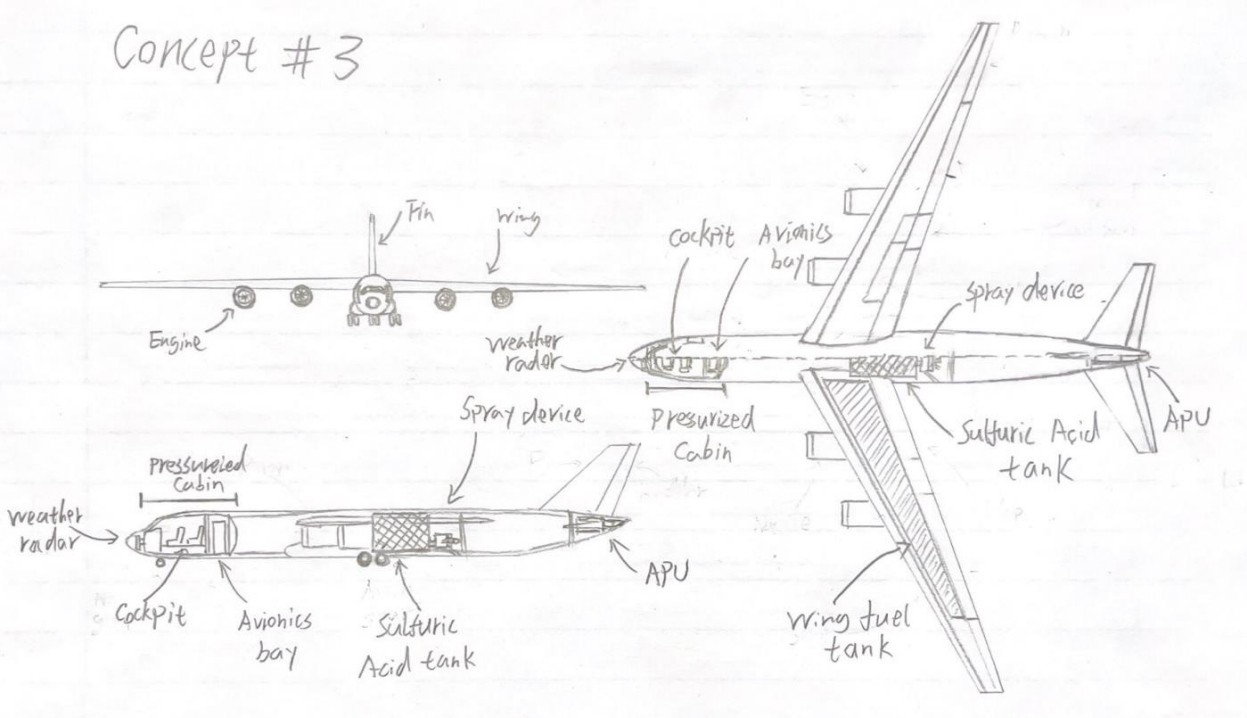

Figure 1-7: Concept sketch of internal layout of configuration 3.

Two more concepts are shown in Figure 1-8 and Figure 1-9, with similar configurations. Both concepts feature dual wing-integrated engines with slightly different wing designs. Both wings have similar aspect and taper ratios, however concept four has significant wing sweep with engines mounted at the middle of the wing, whereas concept five has no sweep and engines mounted at the root of the wing, adjacent to the fuselage. The integrated engine design and reduced wetted area decreases the total drag on both aircraft. The high-sweep configuration is best suited for higher speeds, whereas the sweepless wing design performs better at lower speeds. Integrating the engines into the wings also obstructs the placement of any internal fuel tanks stored in the wing. The design also makes engine maintenance more difficult, and limits the powerplant selection due to the strict dimension requirements needed to fit inside of the wing.

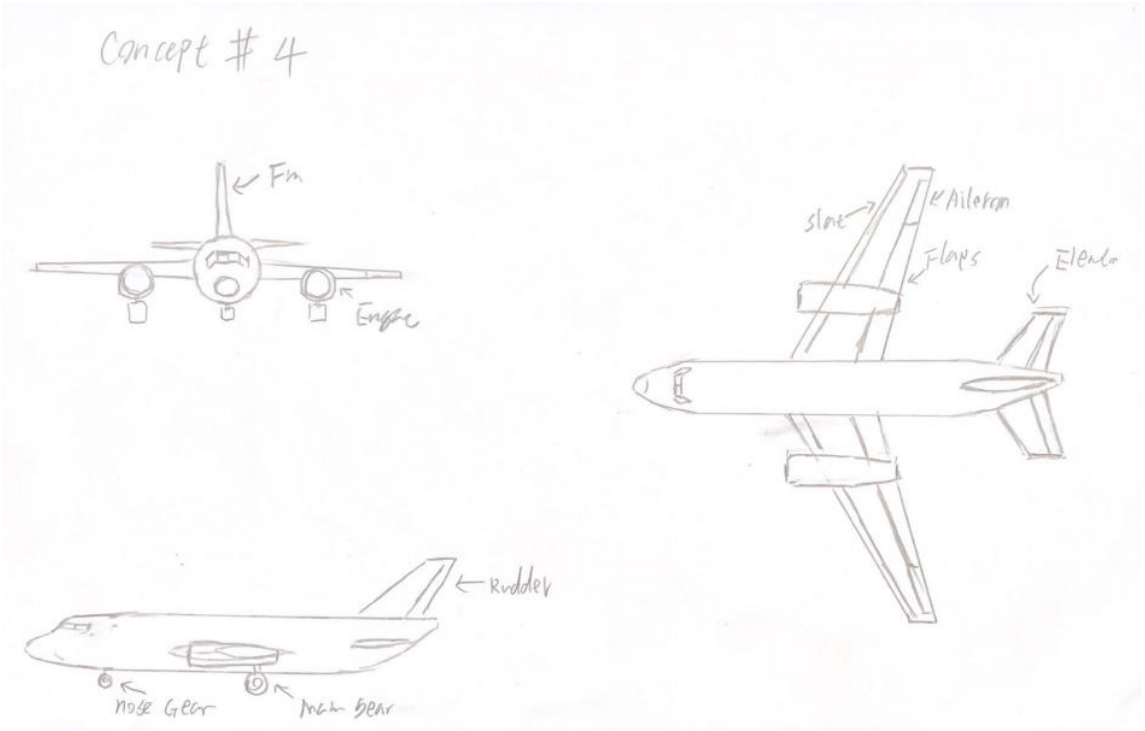

Figure 1-8: Concept sketch of configuration 4.

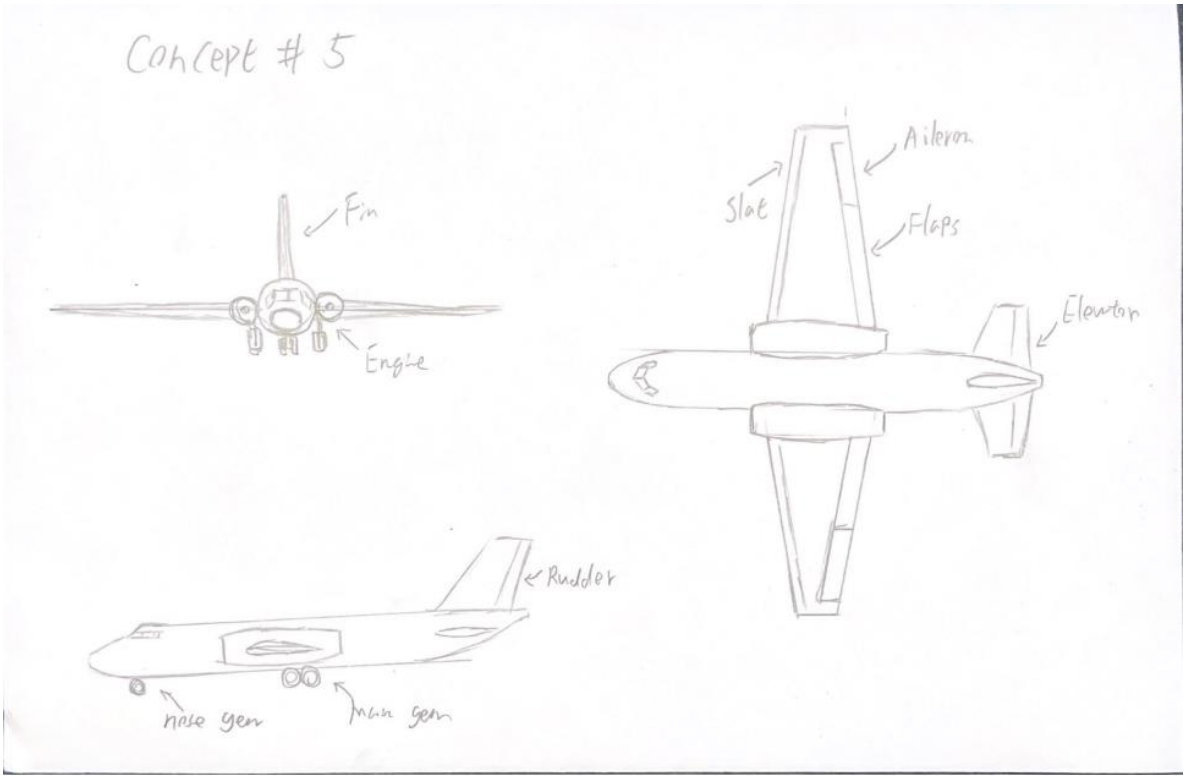

Figure 1-9: Concept sketch of configuration 5.

1.4 Concept Evaluation and Selection

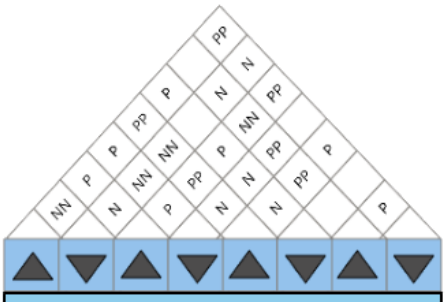

			Engineering Challenges										
			SIZE OF AIRCRAFT	DRAG	LIFT CAPABILITY	PRODUCTION COST	POWER	WEIGHT	ALTITUDE	OPERATING COST	OUR DESIGN	COMP 1	COMP 2
Customer Requirements	Importance 1-5												
FAST	2	9.09	3	9	3	9	9	9	3	9	2	4	1
EFFICENT	4.5	20.45	3	9	9	9	3	3	1	9	4	2.5	4
RELIABLE	4	18.18	1			1	3			3	3.5	2	3.5
PAYLOAD	5	22.73	9	1	9	9	9	9	3	9	2.5	2	3.5
INEXPENSIVE	5	22.73	3	3	3	9	9	9	1	9	3.5	1.5	4
CRUISE ALTITUDE	4.5	20.45	1		9	3	9	9	9	3	4	4	2.5
RANGE	3.5	15.91	1	9	9	3	3	9	3	9	2.5	2.5	4
SUM	22	100.00	4.16	5.00	8.11	8.02	8.39	8.80	3.70	9.34		55.52	
			7.49	9.01	14.61	14.45	15.10	15.84	6.67	16.82			

Figure 1-10: House of Quality for SADIE-65.

Based on customer criteria, the desired qualities for the aircraft include speed, efficiency, reliability, payload capacity, cost-effectiveness, cruise altitude, and range. Based on certain assumptions and the requirements outlined in Table 1-1, the most valued aircraft qualities include efficiency, cost, cruise altitude, and payload as the crucial aspects for the design of the aircraft, with speed being of marginal importance. The engineering challenges involved in this project include typical challenges in aircraft design, such as sizing, drag reduction, lift capability, production and operating costs, power, weight, and altitude. The QFD matrix analysis in Figure 1-10 indicates that solving challenges related to lift capability, power, weight, production and operating costs are of the most importance. From this standpoint, design efforts should be focused on optimizing lift capability and power while minimizing both the weight and cost in the development of the aircraft.

The aircraft concepts presented earlier in Section 1.3 will be evaluated based on the above criteria determined in the HQ matrix. Table 1-3 summarizes some of the major pros and cons of each concept discussed above.

Table 1-3: Pros and cons of selected aircraft configurations presented in Section 1.3.

Concept No.	Pros	Cons
1	• Small, compact – low MTOW, easier storage • Based on similar aircraft capable of flying at high altitudes • Swept wing allows for faster speeds • High aspect ratio for high span efficiency (+winglets)	• Inclusion of internal payload tank forces CG too far aft • Cruciform tail-potential "deep stall" • Small wing area to produce sufficient lift at high altitudes • Resembles different class of aircraft
2	• High aspect ratio • Larger wing area for more lift	• Large; heavy MTOW, greater fuel consumption due to thrust requirement • Resembles different class of aircraft-looks too much like a commercial airliner • Limited engine upgrade capability
3	• Shoulder-wings increase wing clearance • Fuselage more accessible, easier inspection and maintenance Resembles typical design of similar class aircraft • Lower risk of foreign object damage (FOD) due to high engine clearance	• Large; heavy MTOW, greater fuel consumption due to thrust requirement • Improved roll stability from shoulder wings
4	• High aspect ratio • High sweep angle reduces critical Mach number	• Not suited for low-speed flight • Limited options for powerplant selection
5	• High aspect ratio and moderate taper ratio increase span efficiency	• No wing sweep-lower speeds • Limited options for powerplant selection

Among the options considered, the third configuration presented in Figure 1-6 emerged as the preferred choice over the other four concepts. Due to the dual aft-mounted engine design, the

first configuration encounters challenges with weight distribution, exacerbated by the placement of the heavy payload in a relatively short fuselage, forcing the payload tank to be located uncomfortably close to the cockpit. The second configuration features a low-wing design and closely resembles a commercial airliner. However, this concept faced limitations in engine size and upgrade capability due to the minimal clearance between the wing and the ground. This problem was solved in the third configuration, where the wings were moved to the top of the fuselage to increase the wing-to-ground clearance. Concepts four and five provide unique benefits such as increased speed and drag reduction, however they are unique designs which pose potential issues further into the design process. There is also a lack of documentation of similar configurations due to the unique nature of the design, whereas concepts 1-3 are configurations seen in use extensively in aviation.

The shoulder-wing design provides ample space for engine upgrades or replacements, such as accommodating larger diameter engines for future enhancements. With a moderate sweep angle, the aerodynamic center consistently remains behind the center of gravity, ensuring positive or neutral stability. This ensures that either with or without payload it will still remain within the CG envelope. This design feature contributes to stable flight at high altitudes and better high-speed performance due to an increase in the critical Mach number. The high aspect ratio provides better performance during high altitude flight, making the aircraft easier to control while reducing the cruise speed by generating more lift at higher altitudes due to improved aerodynamic efficiency. This design also reduces the landing gear height, decreasing dead weight on the landing gear system and enhancing reliability through a simpler design. The inclusion of retractable gear also improves aerodynamic performance by decreasing drag.

Opting for the shoulder-wing configuration not only reduces the likelihood of foreign object damage (FOD) during takeoff and landing, but also allows the under-wing engines to maintain the center of gravity (CG) in the middle of the aircraft, thereby enhancing overall stability during the whole flight. The quad engines with low bypass ratio ensure acceptable engine performance during high altitude flight. In terms of fuel storage, the fuel tank is positioned in the main wing and center of the fuselage, while the payload tank is situated in the fuselage behind the main wing. This placement enhances the spray range and minimizes the risk of surface corrosion along the bottom of the fuselage.

1.5 Concept Proposal and Reflective Note

The preparation of the concept proposal document and initial stages of conceptual design provided some good insight into the actual steps that go into the conceptual design process of a new aircraft, and what would be expected in the industry. It also served as a good introduction to learning about the numerous regulations for certification by the FAA. One important lesson to be learned is that the process is iterative, so steps should be taken to ensure that calculations

and designs are organized and presented nearly, so that referencing previous work is straightforward and time is not needlessly wasted attempting to make sense of unorganized documents. Based on the feedback provided, it is also wise to not assume primary dimensions and parameters based on concept sketches and existing data before any actual design work has been done. Values should be reported only when sufficient design work has been completed and the numbers can be properly justified.

2 INITIAL SIZING

2.1 Weight Analysis

The mission profile for the primary payload-dispensing mission is a simple cruise mission profile, shown in Error! Reference source not found.. The five main mission segments consist of the following: (1) taxi and takeoff, (2) climb, (3) cruise, (4) descent, and (5) landing. Performance parameters optimized for the cruise segment of the mission are listed in Table 2-1. Upon the completion of takeoff, the aircraft will climb to a cruise altitude of 65 000 feet in under 60 minutes. Once at altitude, the cruise segment begins. At this point, the aircraft will cruise for 400 nautical miles at a true airspeed of 400 knots, or Mach 0.70, at a constant altitude. During this time, the payload will be dispensed at a continuous rate until completion of the cruise leg. Once the payload has been fully dispersed into the atmosphere, the plane will descend over the next 45 minutes, followed by landing. The entire duration of the mission is just under 3 hours. The selected SFC is the value at cruise for the RR TAY-611 turbofan engine.

Table 2-1: Preliminary design parameters for the simple cruise mission.

Parameter	Value	Units
Cruise altitude	65 000	ft
Cruise range	400	nm
Cruise speed	400	KTAS
SFC	0.69	lb_f/lbf.hr
Crew Weight	800	lb_f
Payload Weight	30 000	lb_f
Time-to-climb	≤ 60	min
Time-to-descend	≤ 45	min
Engine cruise thrust	27 700	lb_f
Aspect ratio	8.04	-
Lift-to-drag ratio	13.6	-

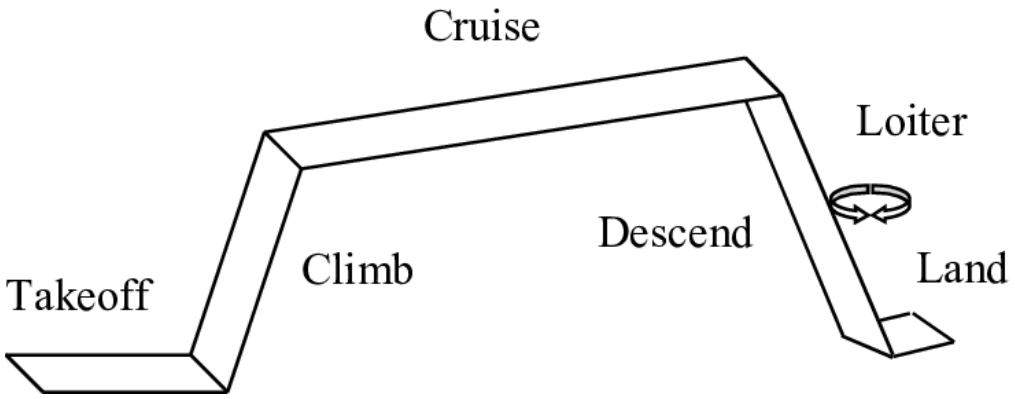

Figure 2-1: The simple cruise mission profile [8].

The sizing analysis that follows provides an estimate for the design gross weight of the aircraft using simple relations for each mission segment in Figure 2-1. The weight analysis process is briefly described below. It is an iterative process, however only the final iteration is presented for simplicity. The methods used can be found in more detail from [9].

To begin the analysis, an arbitrary design gross weight is selected from a range of typical historical values for similar aircraft. These values have been gathered and presented in Table 2-2, along with their respective empty weight fractions. Using the data from this Table, a plot of empty weight fraction vs the logarithm of gross weight was created and is presented in Figure 2-2. By fitting a linear trendline to the data points and matching the predicted gross weight to the trendline, the empty weight fraction can be approximated for the given gross weight.

Table 2-2: Historical empty weight fractions of similar aircraft.

Aircraft	W_0 (lb_f)	W_e/W_0
Boeing 727-100 [10]	169 000	0.519
Trident B3 [11]	107 000	0.553
McDonnell Douglas DC-9 [12]	97 000	0.542
Bombardier Global 7500 [13]	114 850	0.537
Gulfstream G650 [14]	99 600	0.542
Gulfstream V [15]	90 500	0.510
Bombardier Global Express [16]	92 500	0.550
Dassault Falcon 7X [17]	70 000	0.523
Boeing 737-600 [18]	144 500	0.555
Airbus A318 [19]	150 000	0.581
Boeing B-47 [20]	133 030	0.601
Boeing B-52 [21]	265 000	0.698
Rockwell B-1 [22]	326 000	0.589

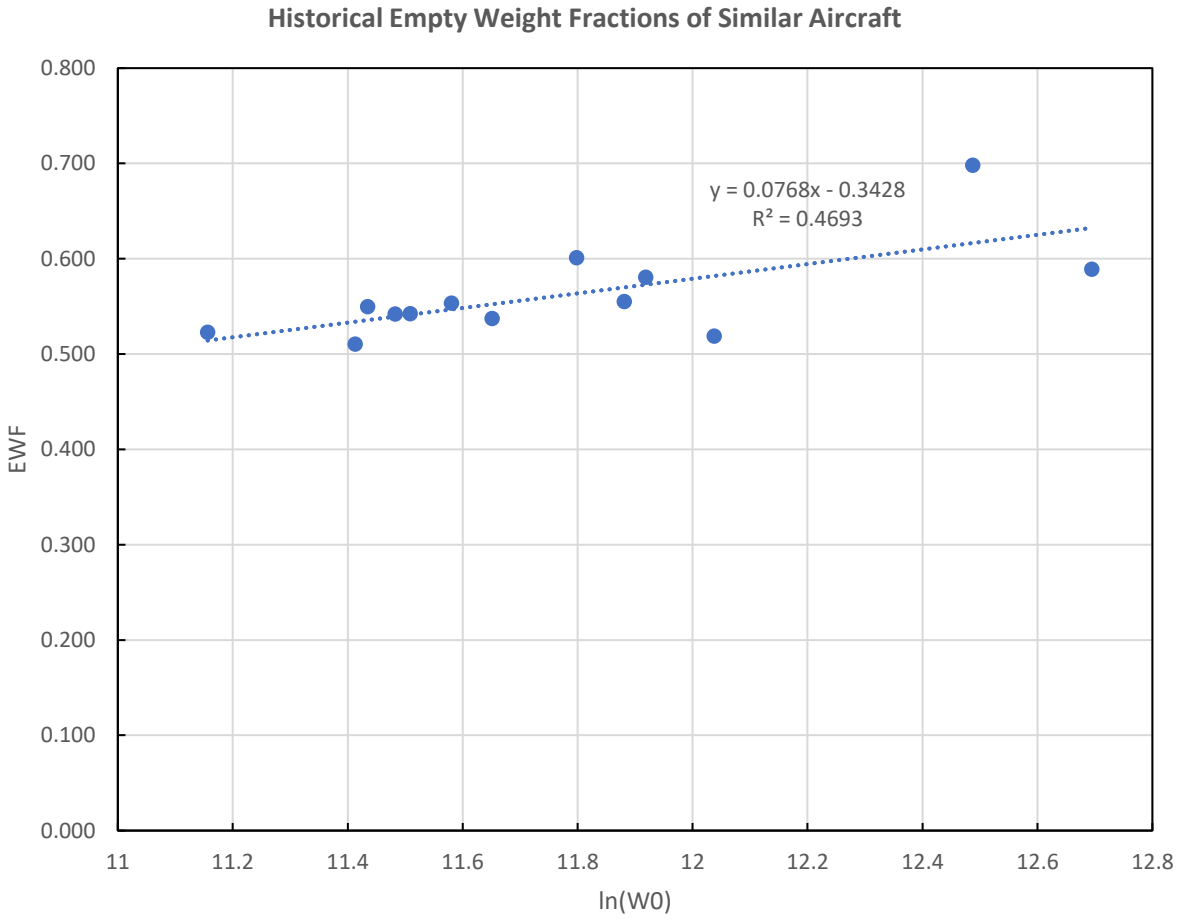

Figure 2-2: Empty weight fraction relations for similar aircraft.

After determining the empty weight fraction, the fuel weight fraction is determined. This value is obtained by first computing the product of each weight fraction for each individual mission segment, which provides the final landing weight of the aircraft, which is equal to the sum of empty and crew weights. The difference between the starting takeoff weight and the final landing weight is the amount of fuel burned to complete the mission, dividing by the gross weight yields the fuel weight fraction. However, due to the unique nature of the payload delivery for this particular mission, the loss of payload must be accounted for when determining the fuel weight. Similarly, when determining the weight fraction for the cruise segment, this gradual payload drop must be accounted for on top of the fuel consumption. This was accomplished by determining the weight fractions for several incremental steps of the cruise leg for every certain number of nautical miles covered. The product of all these weight fractions yielded the final weight fraction for the entire cruise leg. The final weight fractions for each mission segment are given in Table 2-3, along with the empty and fuel weight fractions.

To determine the weight fraction for taxi and takeoff, the following equation was used

$$\frac{W_1}{W_0} = 1 - (\Delta t_{taxi} \cdot r_{idle} + \Delta t_{max} \cdot r_{max}) \cdot SFC \quad (1)$$

Where the fraction on the left side of the equation is the weight fraction for the taxi and takeoff mission segment, Δt_{taxi} and Δt_{max} are the times elapsed for engines running at idle and max throttle respectively, and r_{idle} and r_{max} are the thrust-to-weight ratios for idle and max thrust, respectively. To use the equation, the idle thrust was assumed to be 7% of the max thrust, and the values for Δt_{taxi} and Δt_{max} were assumed to be 20 and 1 minute(s), respectively, based on current trends.

The weight fraction for the climb segment is given by the following equation

$$\frac{W_2}{W_1} = \frac{1 - \Delta H \cdot C_t \cdot r_{climb}}{(60) ROC_{avg}} \quad (2)$$

Where the fraction of the left side of the equation is the weight fraction for climb, ΔH is the change in altitude, C_t is the SFC for a turbojet engine, r_{climb} is the thrust-to-weight ratio required for climb, and ROC_{avg} is the average rate of climb. Since the engine thrust and rate of climb decrease with altitude, to obtain a better approximation for the weight fraction equation (2) was applied over finite intervals of 500 ft, from sea level all the way up to the cruise altitude. Over each interval, the thrust at the given altitude was calculated based on the thrust lapse model and used to calculate the rate of climb. Taking the product of all of these weight fractions over each finite interval resulted in the total weight fraction for climb. This method provided a far better approximation for the weight fraction, as assuming a constant rate of climb and thrust at sea level resulted in a grossly overestimated MTOW. The thrust model used, along with calculations for rate of climb are provided in Section 3.

The weight fraction for cruise was given by the Breguet range equation, which is given below, and rearranged to obtain equation (4).

$$R = \int_{W_{i-1}}^{W_i} -\frac{V_\infty \left(\frac{L}{D}\right)}{C_t \cdot W} dW = \frac{V_\infty \cdot \left(\frac{L}{D}\right)}{C_t} \cdot \ln\left(\frac{W_{i-1}}{W_i}\right) \quad (3)$$

$$\left(\frac{W_i}{W_{i-1}}\right) = e^{\frac{-R \cdot C_t}{V_\infty \cdot \left(\frac{L}{D}\right)_R}} \quad (4)$$

Where R is the range, $V\infty$ is the cruise airspeed in KTAS, C_t is the SFC, and $(L/D)_R$ is the best L/D for the best range, which was determined based on the lift curves and drag polars presented in Section 3. The values used in the equation are found in Table 2-1. As stated earlier, due to the fact that the payload weight decreases at a constant rate over the entire cruise leg, this effect is not considered in equation (4). To factor in this drop in payload, a similar method was used to approximate the weight fraction as the method used for the climb weight fraction.

To model the gradual reduction in payload, equation (4) was used over several finite range intervals, where the weight at the beginning and end of each interval would be calculated using this equation, which would determine the fuel burn over each interval. Between each interval, the payload weight was decreased by a constant amount, such that the payload would be at a maximum at the beginning of the cruise leg, and zero by the 400 nm mark. Taking the product of all finite weight fractions provided the total weight fraction for the cruise leg. Using this method allowed for a better approximation of the weight fraction, as less fuel would be required to maintain steady flight as more payload is dropped. Assuming the payload to be constant would overestimate the amount of fuel needed for cruise, and thus would also overestimate the gross weight. For comparison, the weight fraction for cruise without dispensing the payload is also shown in Table 2-3, with values presented both including and not including the payload weight. Comparing the values, it can be observed that without factoring in the payload drop, more fuel is burned which is reflected by the lower weight fraction.

The weight fractions used for the descent and landing mission segments were taken as constant values, based on historical data and current trends. To determine the effect of some of the parameters in Table 2-1 on the final gross weight, a sensitivity study was conducted by varying several of the parameters, and by analyzing the results, it was noted that the selection of parameters made for use in equations (2) and (4) do not have a great effect on the final weight. The full sensitivity analysis is presented in Section 2.2.

Table 2-3: Sizing analysis weight fractions for final iteration.

Weight Fraction	Value
Taxi & T-O	0.992
Climb	0.938
Cruise (No payload drop) $+W_P$	0.951
Cruise (No payload drop) $-W_P$	0.618
Cruise (Payload drop)	0.626
Descent	0.950
Landing	0.990
Total	0.547
Empty Weight	0.539
Fuel Weight	0.143

To determine the empty weight fraction, the following equation was used

$$EWF = Aln(W_0) + B = 0.0768\ln(W_0) - 0.3428 \quad (5)$$

Which is a simple linear relationship used to approximate the empty weight fraction of the aircraft using the design gross weight and the trendline fitted to the data points in Figure 2-2. Multiplying the empty weight fraction by the gross weight yields the empty weight. To determine the fuel weight fraction, the product of all mission weight fractions was calculated to determine the final aircraft weight after landing. The final weight plus the payload weight, subtracted from the gross weight is the amount of fuel burned to complete the mission. Dividing by the gross weight yields the fuel weight fraction.

$$W_F = W_0 - (W_5 + W_P) \quad (6)$$

$$FWF = \frac{W_F}{W_0} = 1 - \frac{W_F + W_P}{W_0} \quad (7)$$

Using the weight fractions from Table 2-3, the aircraft weights at each point of the mission are reported in Table 2-4.

Table 2-4: Weight upon completion of each mission segment.

Mission Segment	Weight at End of Segment (lb_f)
Taxi & T-O	96 040
Climb	90 056
Cruise	56 343
Descent	53 526
Landing	52 990

Using all of the data from above, the design gross weight, as well as other important weights are listed in Table 2-5. A full example of sample calculations using equations (1) – (7) can be found in Appendix A. The sizing analysis is an iterative process which requires multiple iterations to calculate a final gross weight, for this reason only calculations for the final iteration are provided for conciseness.

Table 2-5: Summary of aircraft weights in lb_f.

Design gross weight	96 804
Empty weight	52 190
Fuel Weight	13 814
Payload weight	30 000
Crew weight	800

Figure 2-3 presents a payload-range study which was conducted with varying payloads and quantities of fuel. The maximum payload for the aircraft is 30 000 lb, with a maximum fuel capacity of 20 000 lb. The study shows the trade-off between payload and fuel, and the effect this has on the cruise range. The leftmost point, point A, carries the maximum amount of payload with no fuel, which thus has a range of zero. To the right is point B, or the design point, which meets the required mission specifications, requiring 13 814 lb of fuel at MTOW and a payload weight of 30 000 lb. Point C is located down and to the right, which shows the range at maximum fuel capacity and partial payload, still at MTOW. At this point payload capacity is traded for fuel. Finally, point D carries maximum fuel with no payload, exhibiting the longest cruise range. A tabulated version of the data points from the plot is shown in Table 2-6.

The range was calculated using the Breguet equation for (3), with all other parameters held constant while varying the weight fractions. The coordinates for point B are based off of the aircraft requirements, with points C and D being approximated using estimated values for the fuel burned during cruise and the extra fuel afforded by the reduction in payload weight. All of the extra fuel was considered to be used during cruise, with the fuel consumption for all other mission segments remaining constant. In actuality, the fuel consumption for each segment would vary, however, to simplify the calculations they were assumed to remain constant. Recalculating the fuel burned for cruise at these different points would each require another separate sizing analysis, with the given payload and fuel weights.

Table 2-6: Tabulated data for payload-range plot (Figure 2-3).

	Cruise Range (nm)	**W_P**
Point A	0	30 000
Point B	400	30 000
Point C	1 050	23 814
Point D	1 422	0

The plot shows that if extra range were desired by the customer, the total payload capacity can be reduced in favor of carrying more fuel, while still remaining at the MTOW of 96 804 lb.

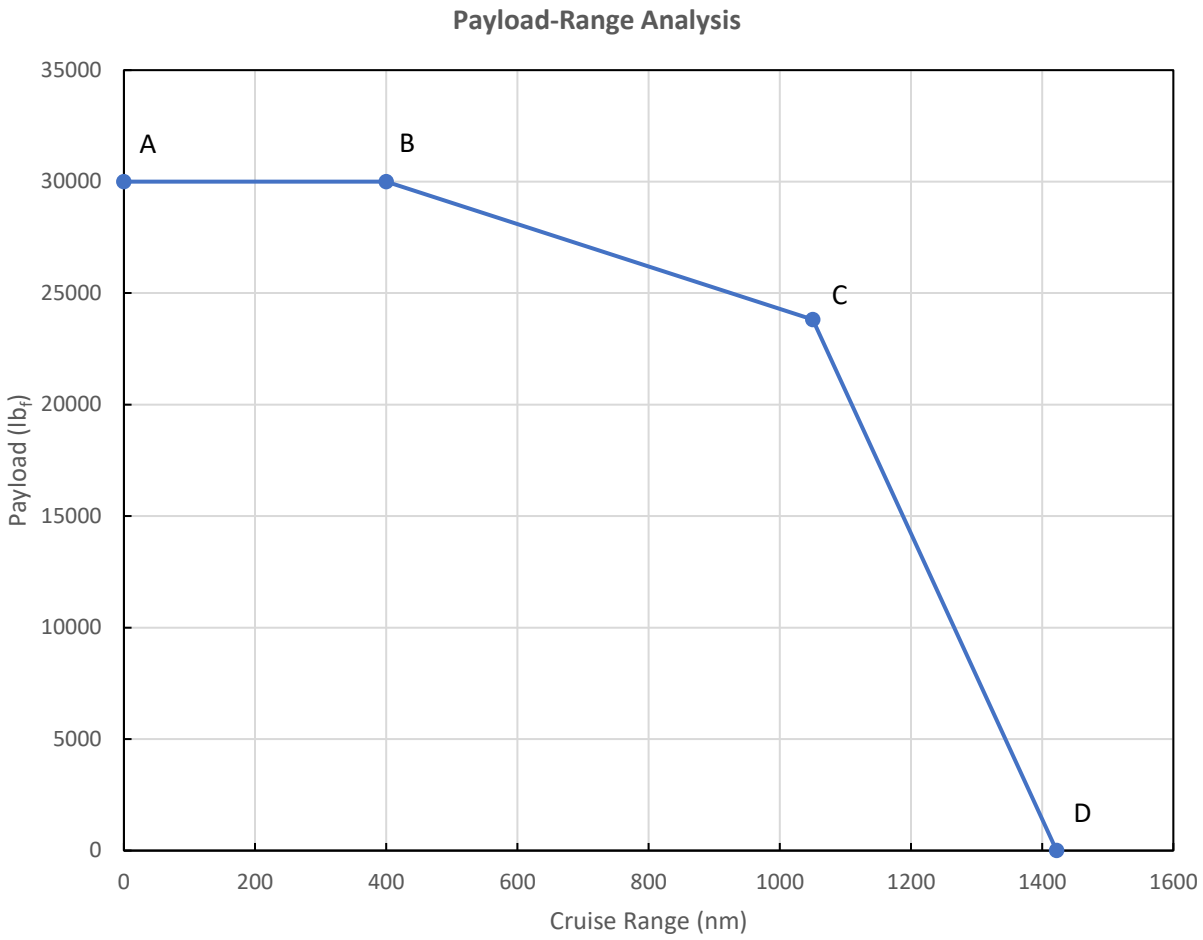

Figure 2-3: Payload-range analysis.

2.2 Sensitivity Studies

A sensitivity analysis was performed in order to analyze the sensitivity of the design gross weight to several different parameters. The analysis was conducted by calculating the gross weight as a function of only one varying parameter at a time. Each parameter was modified over a fixed range of percentages of its initial value. By a quick inspection of Figure 2-4, it can be easily identified that the gross weight is most sensitive to the empty weight fraction, thus it was crucial that sufficient data was collected in Table 2-2 to generate an accurate relationship between the empty weight fraction and gross weight in order to obtain a valid estimation of the aircraft gross weight. Second to the EWF, the design gross weight is most sensitive to a decrease in the lift-to-drag ratio. For this reason, the selection of this parameter may be a potential source of error, depending on the lift and drag approximation methods and the software used to generate these curves. The remaining modifiable parameters have a relatively insignificant impact on the final

weight, however a lower SFC may result in a slightly lighter aircraft. Different SFCs for different mission segments could potentially influence the gross weight, as the engine SFC was assumed to be constant for the entire duration of the mission. Range and payload data provide little use, as they are fixed values as per the requirements outlined in the RFP. Complete tabulated data used to plot Figure 2-4 can be found in Appendix Error! Reference source not found..

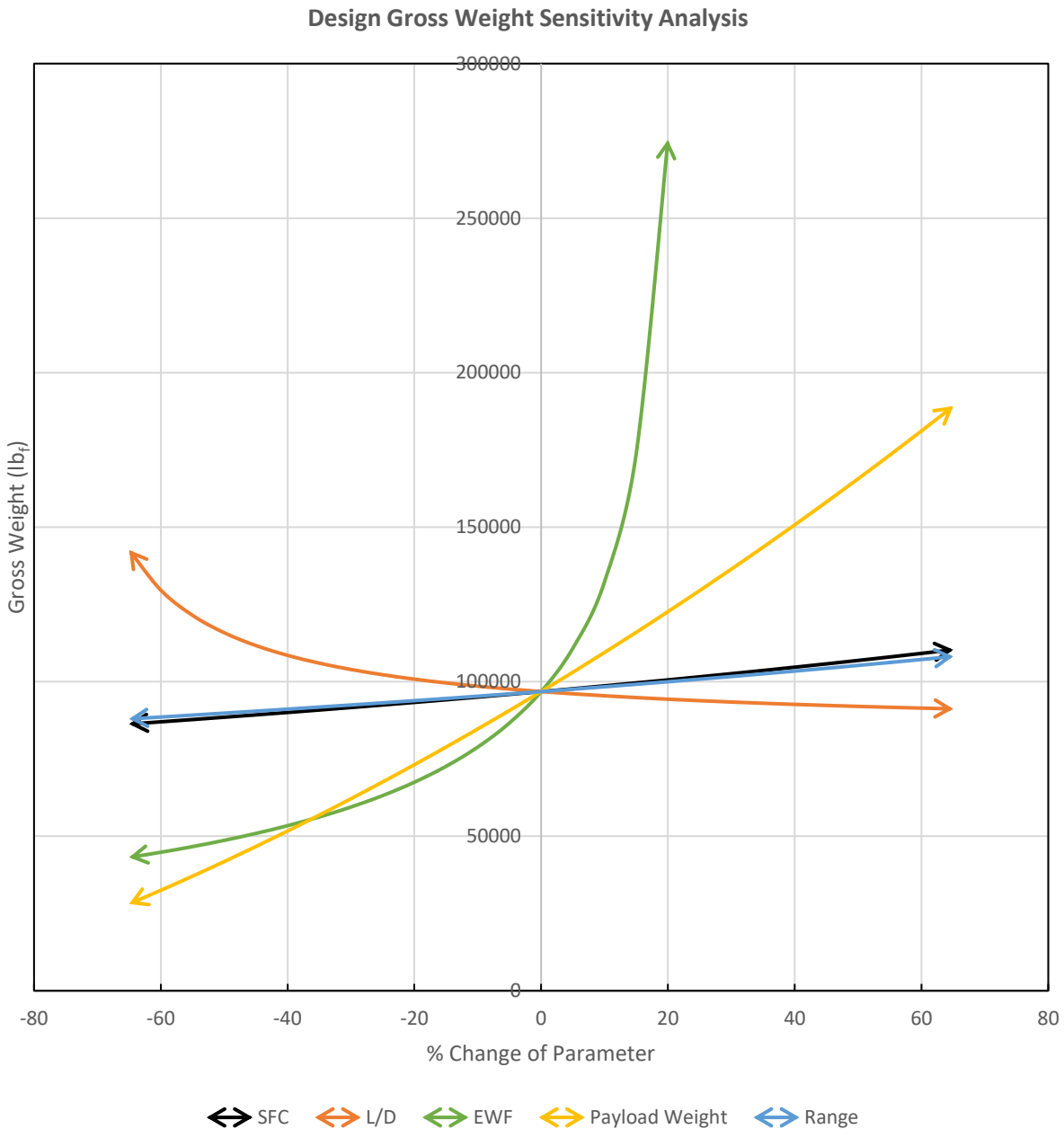

Figure 2-4: Sensitivity analysis on design gross weight.

3 GEOMETRY REFINEMENT AND PERFORMANCE

3.1 Geometry Selection

3.1.1 Wing Configuration

When designing the main wing, the location of the wing fuel tank and payload tank is mainly considered. The location of the payload box is restricted because the low- and mid-wing design reduces the available space inside the fuselage. In the end, a shoulder-wing design was chosen, although it was not conducive to the design of the landing gear. The final preliminary wing design selected a high wing with a small sweep angle, a relatively large taper, and a downward angle of 8 degrees. Two different airfoils, NACA 2412 at the root and NACA 0012 at the tip were chosen for the airfoil of the wing, which can reduce the weight of the wing and have better aerodynamics. Finally, this design can have a higher aspect ratio to increase lift and optimize the aircraft's high-altitude performance as much as possible. A summary of the main wing geometrical parameters is presented in Table 3-1.

Table 3-1: Primary wing parameters.

Parameter	Symbol	Value	Units
Aspect ratio	AR	8.04	-
Taper ratio	λ	0.457	-
Sweep angle	Λ_{LE}	7.53	°
Span efficiency	e	0.8809	-
Airfoil (Root)	-	NACA 2412	-
Airfoil (tip)	-	NACA 0012	-

3.1.2 Tail Configuration

When designing the tail wing, the conceptual design included a T-shaped tail wing, cross-shaped tail wing and conventional tail wing. V-tails were not considered because they are typically only used on small aircraft and would increase the complexity of flight control. Through weight, cost and efficiency analysis, the conventional tail wing was finally selected from T-shaped, cross-shaped and traditional tail wings. Although high-mounted wings usually use a T-shaped tail to prevent the tail from being covered by the wake generated by the wing at high angles of attack, due to the large downward angle of the main wing, the main airflow will be directed downward to reduce the impact on the tail. A T-tail is another option, but a T-shaped structure requires a stronger tail structure, which adds extra weight. In the end, after considering various factors, a

traditional rear wing was chosen. A summary of the tail geometrical parameters is presented in Table 3-2.

Table 3-2: Tail geometrical parameters.

Parameter	Value	Units
Horizontal tail angle	18.93	°
Vertical tail angle 1	66.85	°
Vertical tail angle 2	36.73	°
Horizontal tail size	3.79/1.55 x 5.81	m
Vertical tail size	4.07 x 5.74/1.6	m
Airfoil	NACA 0012	-

3.1.3 Fuselage Shape

In the original design of the aircraft, a cylinder was chosen as the fuselage shape. This is due to flight altitude and structural design. Because the entire cockpit needs to be pressurized, a round shape is the best way to reduce local stress points, thereby increasing the aircraft's life and reducing structural weight. Regarding the fuselage length, although the design load does not require much space, to ensure the control performance and safety of the aircraft (the main wing will be too close to the tail wing, which will affect aircraft control). Secondly, the length of the fuselage will have an impact on the CG position of the aircraft. Based on the analysis of structure and load, the fuselage length was finally selected as 27.8m.

3.1.4 Engine Selection and Placement

Engine selection/location needs to consider the impact on the aircraft's center of gravity, the load-bearing capacity of the structure, and the failure of one engine. According to the design of the aircraft's center of gravity, the engines are placed under the main wings, with the center of gravity slightly forward (to balance the weight of fuel and payload). Positioning the engine close to the center of the fuselage can reduce the moment generated when a single engine fails and ensure that the vertical tail is balanced within the range. Additional benefits of placing the engine under the main wing include the ability to use gravity to refuel the engine when the fuel pump fails, and ease of engine maintenance. Based on these results, the design under the main wings was finally chosen.

3.1.5 Landing Gear

Due to the design of the fuselage and wings, tricycle landing gear was the only landing gear design available. SADIE chose a lower landing gear height. The disadvantages of this design include small ground clearance and easy tail strike. Usually, the landing gear of an aircraft requires a greater height to ensure that there is no tail strike during takeoff. However, the large angle of the main wing allows the aircraft to take off without too much rotation, thereby reducing the requirement for maximum takeoff angle. The advantage of a lower-height landing gear is that it reduces dead weight and reduces the requirements for the internal space of the fuselage when the landing gear is retracted.

3.1.6 Door / Windows

Regarding the design of aircraft doors and windows, the design ensures minimal impact on the appearance of the aircraft. Reduced drag is achieved by maintaining a streamlined design. The size of the door is 0.83 x 1.8 m and has a small window to observe external situations (e.g. emergencies). The size of the main window of the aircraft ranges from 0.45 to 0.78 meters (the specific size can be found in Figure 4-2) and has a field of view of 23-30 degrees from the pilot's perspective (depending on the head position). This ensures visibility during takeoff, cruise, and landing, reducing the likelihood of accidents.

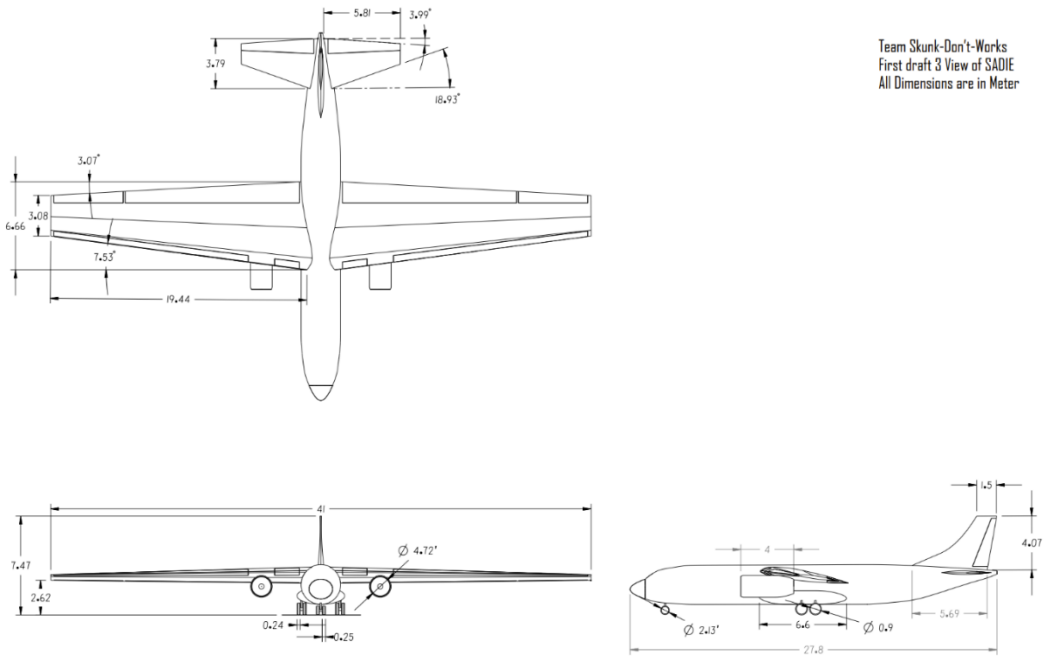

Figure 3-1: Preliminary 3-view drawing of SADIE-65.

3.2 Lift Curve and Drag Polar

Using XFLR5, the two NACA 2412 and 0012 airfoils used for the wing were simulated at various different Reynolds numbers to obtain the drag polars and lift curves presented in Figure 3-2 and Figure 3-3, respectively. A legend for the two figures is provided in Table 3-3. Each airfoil was simulated with same Reynolds number required for the wing analysis in order to avoid convergence errors while running the analyses.

Table 3-3: Legend for 2D lift curves and drag polars.

Line Style	Airfoil
Solid-Yellow	NACA 2412
Solid-Blue	NACA 0012
Dashed-Black	NACA 2412 w/ flaps (TO)
Dashed-Green	NACA 2412 w/ flaps (LDG)

Both airfoils have similar aerodynamic properties with similar stall characteristics. The drag polars are fairly similar as well, however the NACA 2412 airfoil has a slightly better maximum lift-to-drag ratio at similar Reynolds numbers to the NACA 0012 foil.

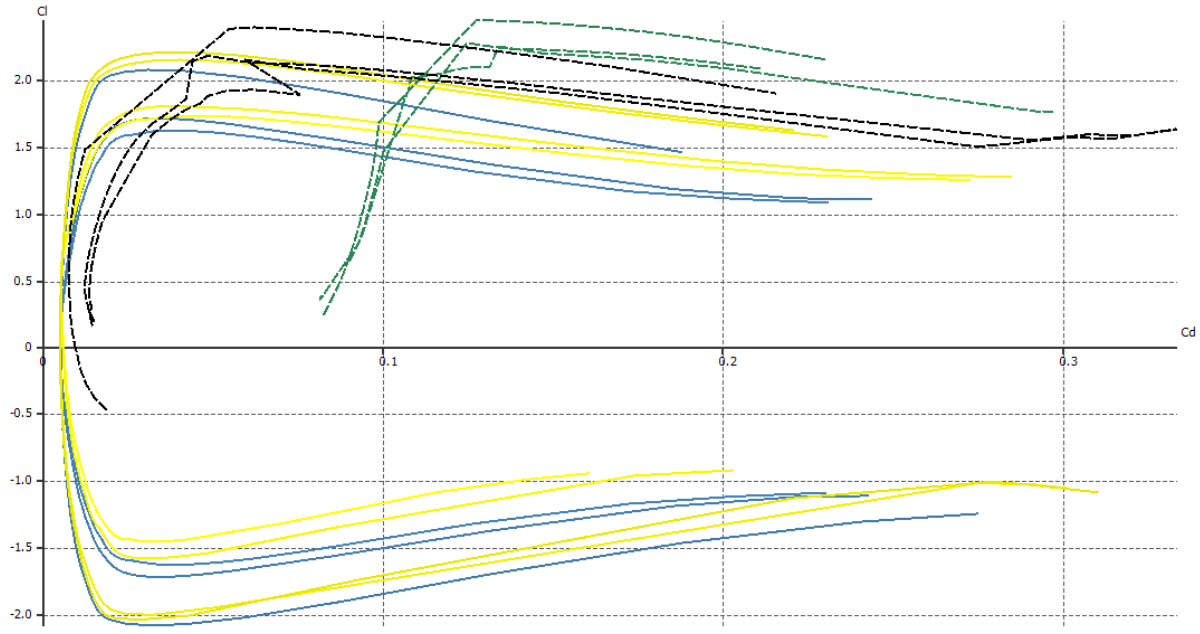

Figure 3-2: 2D drag polar for NACA 2412 and NACA 0012 airfoils at varying Reynolds numbers.

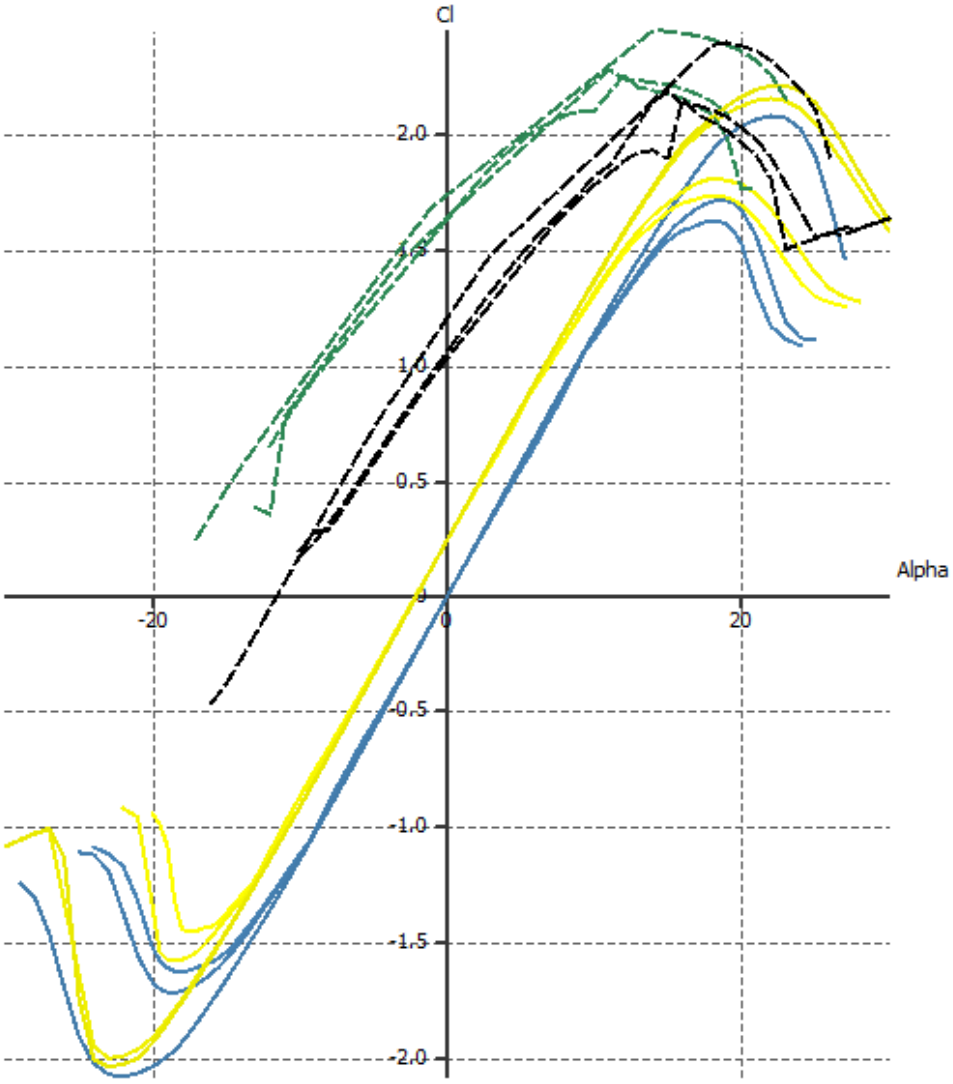

Figure 3-3: 2D lift curve for NACA 2412 and NACA 0012 airfoils at varying Reynolds numbers.

Using the wing geometry from Table 3-1 along with the sizing parameters from Section 3.4, the 3D wing was modeled in XFLR5 and simulated with the appropriate speed and air density at the required cruise altitude. A clean version of the wing without flaps is shown in Figure 3-4, with the NACA 2412 airfoil at the root, and the NACA 0012 airfoil at the tip. In order to obtain the lift curves for the takeoff and landing flap configurations, the wings were also modelled flips flaps at varying levels of deflection. At takeoff, the trailing edge flaps are deflected down by an angle of 25 degrees, and an angle of 45 degrees for landing. 3D models for the wing generated in XFLR5 are shown for takeoff and landing conditions in Figure 3-5 and Figure 3-6, respectively.

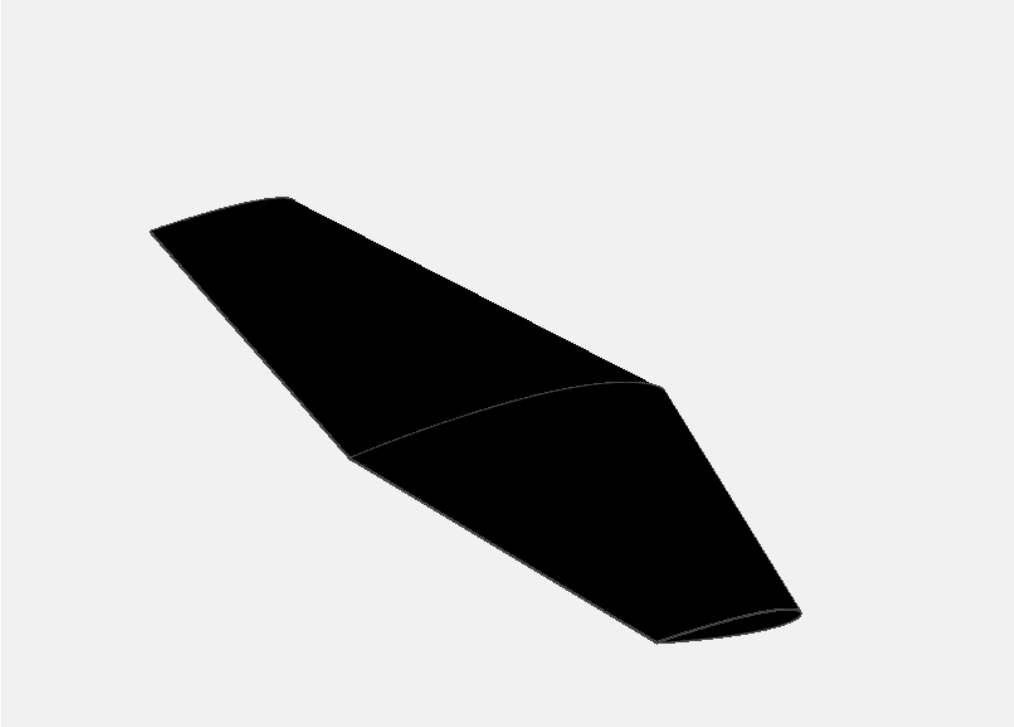

Figure 3-4: Model of clean wing generated in XFLR5.

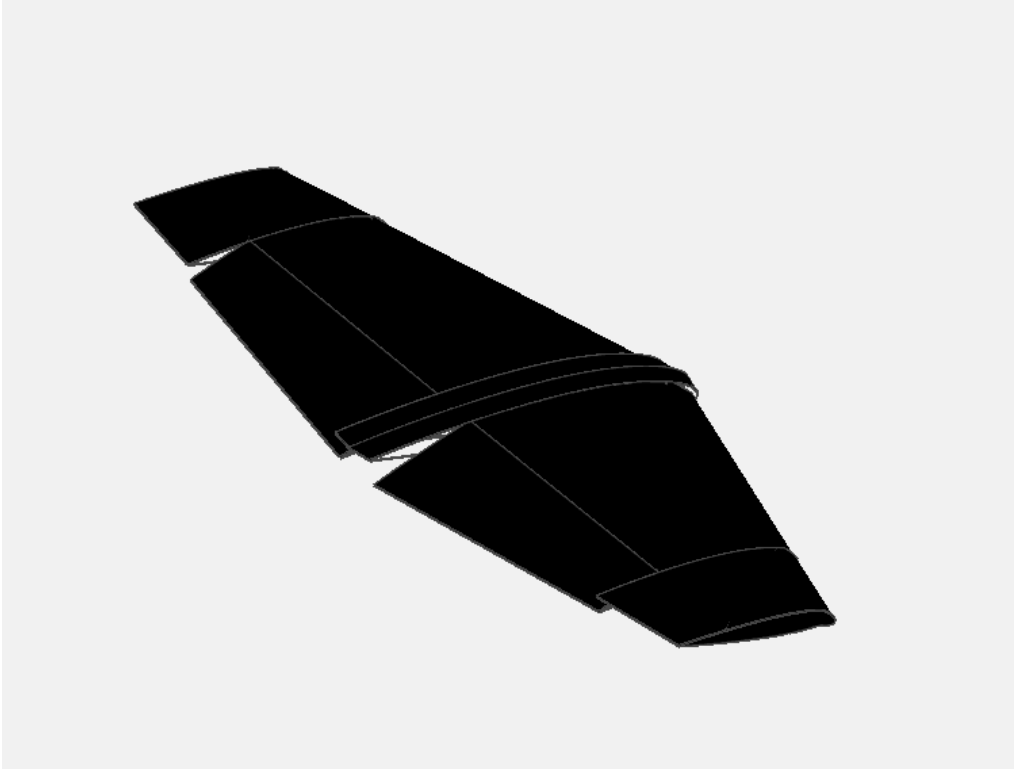

Figure 3-5: Model of wing w/ flaps in takeoff position.

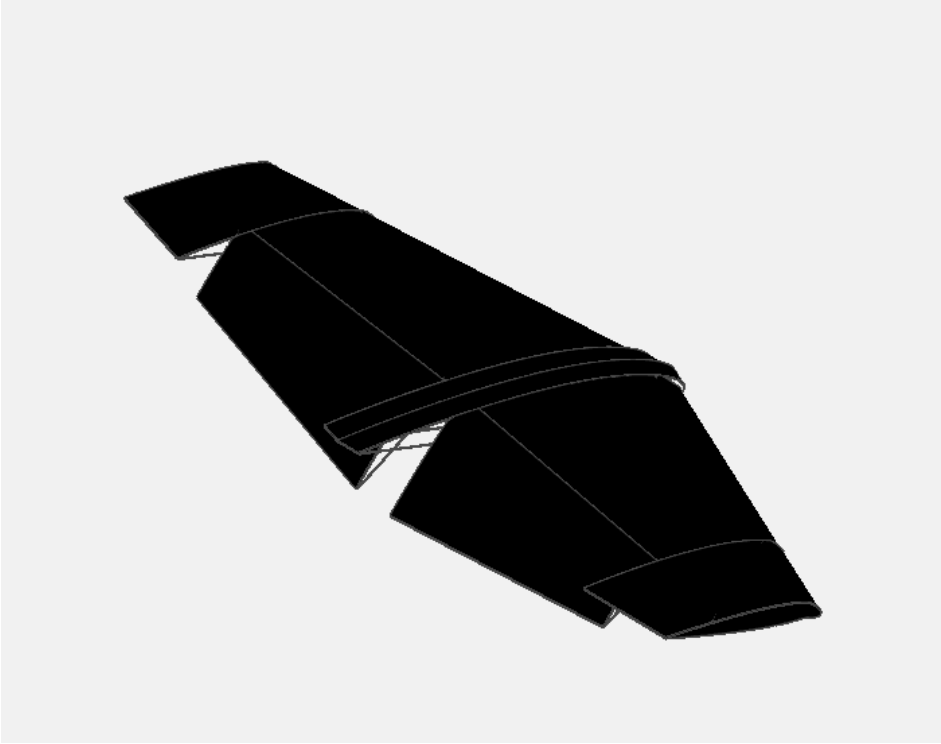

Figure 3-6: Model of wing w/ flaps in landing position.

Using the three different wing models, an analysis was run on each wing in XFLR5 at the appropriate Reynolds number to generate the lift curves and drag polars for each configuration. The lift curves are shown in Figure 3-7. A legend for the plot is presented in Table 3-4.

Table 3-4: Legend for lift cure and drag polar.

Line Colour	Wing Configuration
Cyan	Clean
Blue	T-O flaps
Magenta	LDG flaps

In order to generate sufficient lift during cruise, the following equation was used to determine the minimum lift coefficient.

$$C_{L_c} = \frac{2\left(\frac{W}{S}\right)}{\rho V_c^2} \tag{8}$$

Evaluating equation (8) at the cruise altitude of 65 000 ft and a true airspeed of 400 KTAS, the minimum lift coefficient was determined to be 0.811. At an angle of attack of 8 degrees, the clean wing has a lift coefficient of 0.813. For this reason, the angle of incidence was to set 8°, so that the aircraft can generate sufficient lift without excessive angles of attack during cruise. Due to convergence errors while running the analysis, XFLR5 was unable to plot the lift curve past angles of attack of 12°. However, at this point the slope of the lift curve for the clean configuration begins to slow at the onset of stall. The maximum lift coefficient for a clean wing was thus found to be just under 1.7. The plot also shows the lift curves for the landing and takeoff flap configurations, which each increase the lift coefficient at a zero angle of attack by about 0.4. Key lift curve parameters for all wing configurations are shown in Table 3-5.

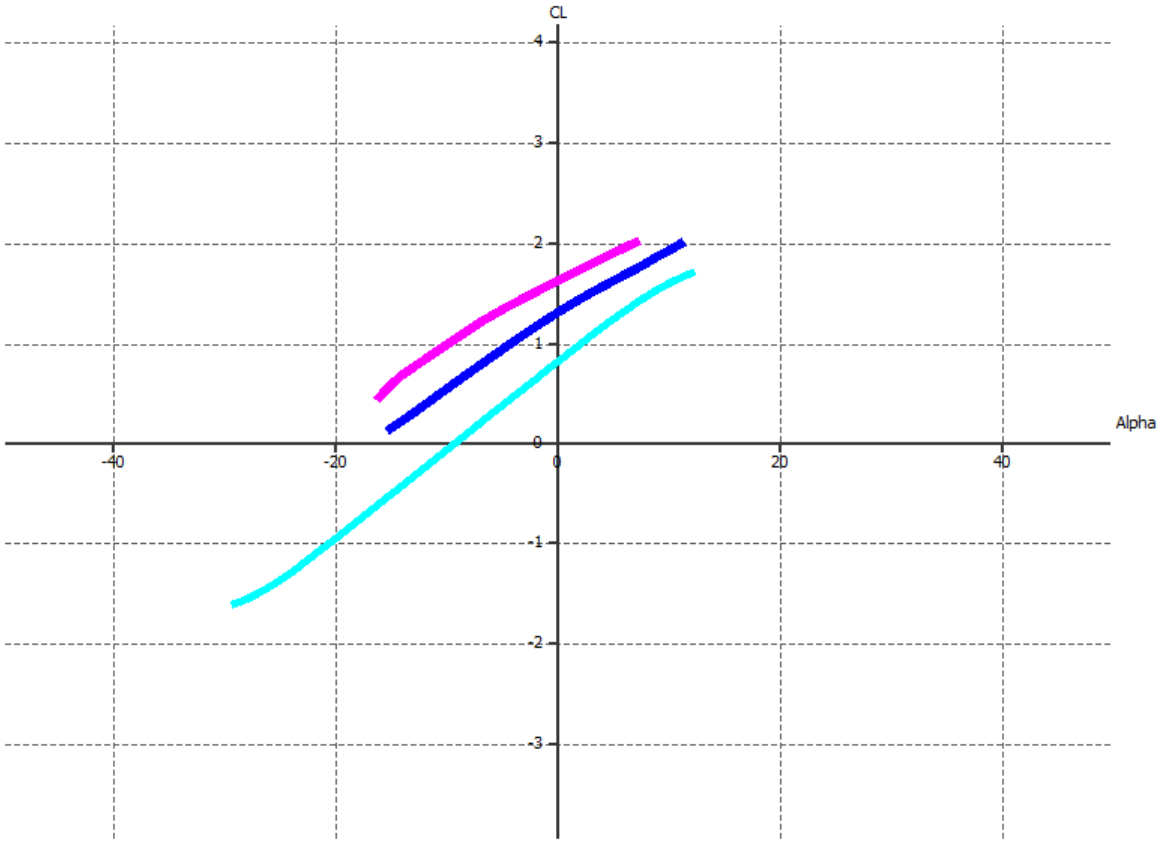

Figure 3-7: Partial 3D lift curve for wing at different flap positions.

Table 3-5: Key lift curve parameters.

Parameter	Value
C_{L0}	0.813
α_{ZL}	-9.5
$C_{L\alpha}$	0.088/°
C_{Lmax} (clean)	1.7
C_{Lmax} (T-O)	2.1
C_{Lmax} (LDG)	2.5

Next, the drag polars for all three wing configurations are plotted in Figure 3-8, using the same legend from Table 3-4. Using the drag polar of the clean wing, several key parameters can be deduced. These values are tabulated in Table 3-6. A plot of C_L/C_D was also generated and included in Figure 3-9. This plot shows the location where the maximum L/D is achieved.

Table 3-6: Key drag polar parameters.

Parameter	Value
C_{Dmin}	0.03
C_{LminD}	~0
AOA at best L/D	-5.5°
C_L at best L/D	0.35
C_D at best L/D	0.010
Max L/D	13.62

Using the values from Table 3-6, the value L/D is calculated as 35, which is also reflected by the peak in the plot of Figure 3-9. However, this value is too high due to the fact that the drag values generated from the analysis only accounts for the drag of the wing, and not the entire plane. For this reason, a minimum drag of 0.03 was selected, primarily based off of historical values of similar classes of aircraft [9]. Using this value, the new equation for L/D can be calculated using the following equation derived from the simplified drag model.

$$\left(\frac{L}{D}\right)_{ma} = \sqrt{\frac{\pi \cdot AR \cdot e}{4C_{D_0}}} = 13.62 \tag{9}$$

Compared to the preliminary estimate of 17.6, the calculated value from above is significantly lower. However, it likely provides a better estimate, as the original L/D was approximated using the aspect ratio and wetted area approximations, along with empirical data. Since the lift

coefficient at the minimum drag is approximately zero, use of the modified drag equation would effectively provide the same result.

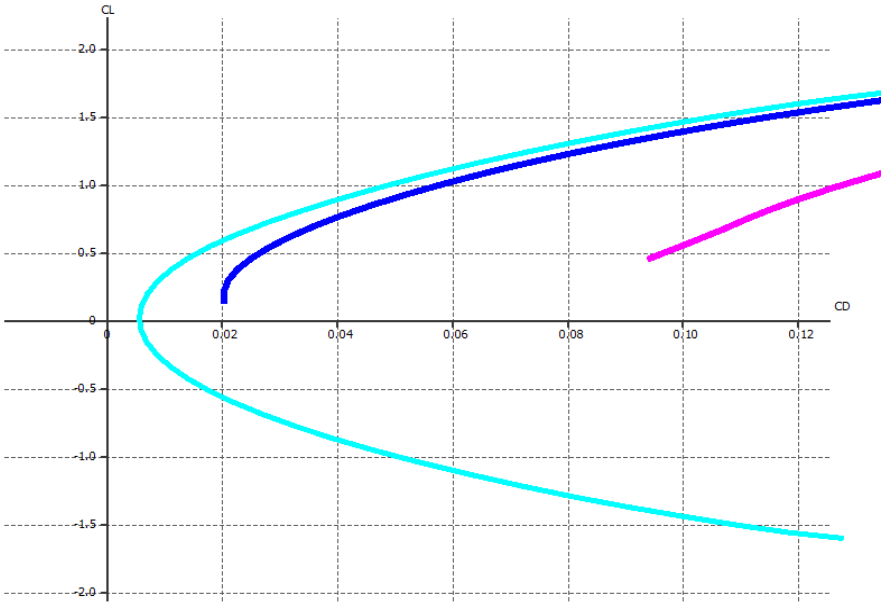

Figure 3-8: Drag polar for wing at different flap positions.

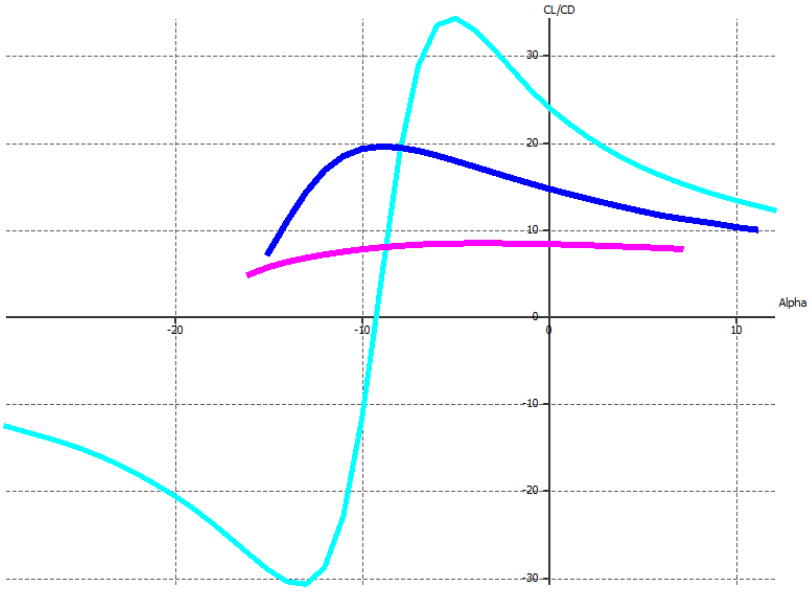

Figure 3-9: L/D ratio at different angles of attack at different flap positions.

3.3 Constraint Analysis

A constraint analysis was performed to determine feasible values for the thrust-to-weight ratio and wing loading. Several constraints were considered, such as stall conditions, takeoff conditions, climb parameters, etc. A full list can be found in Figure 3-10. An atmospheric model was also created so that the air properties at various different altitudes could be referenced and used in calculations. The first two constraints are the stall speeds for both a clean wing and deflected flaps.

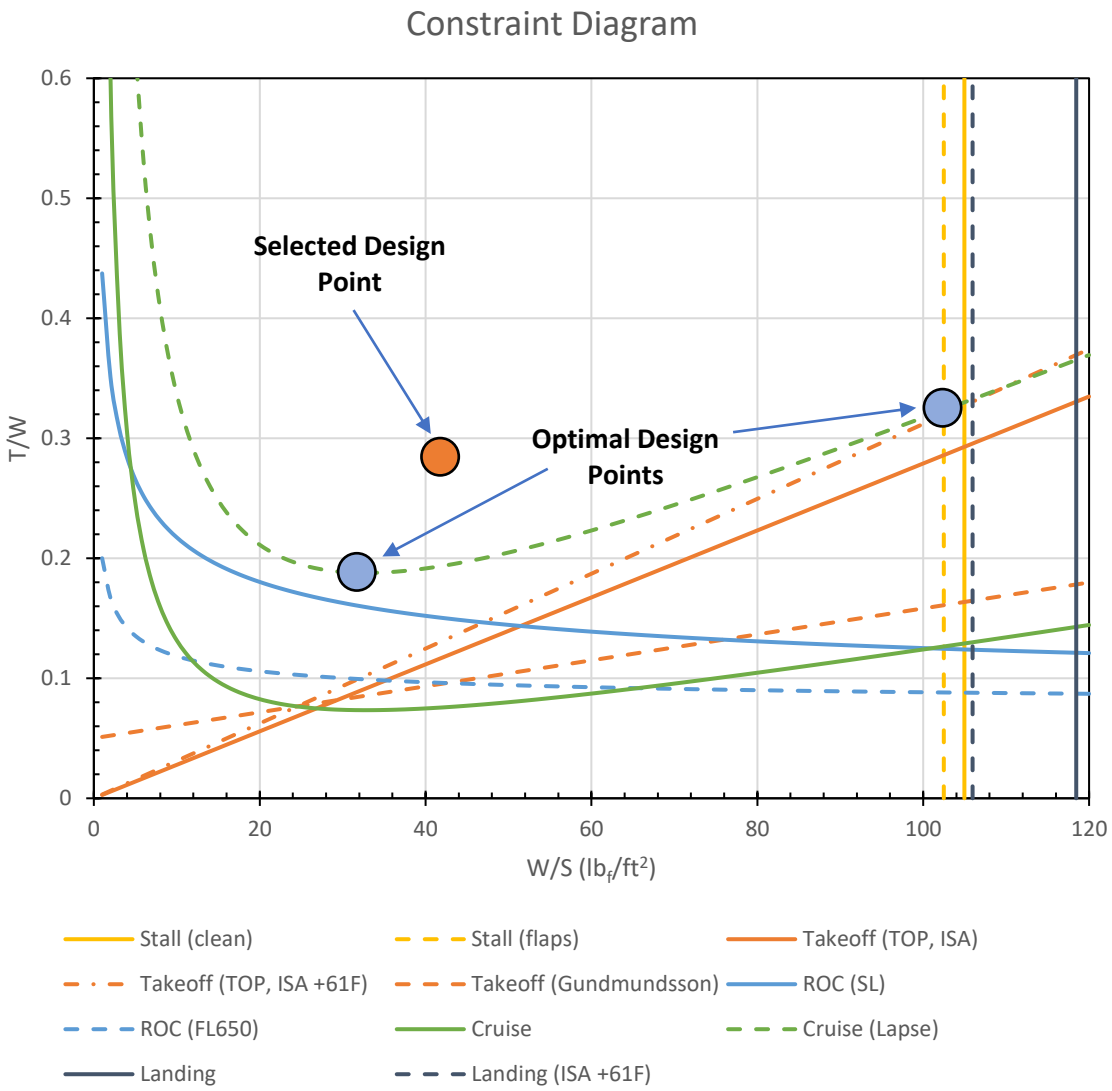

Figure 3-10: Constraint diagram showing optimal and selected design points.

Observation of the constraint diagram shows two different optimal design points, which are labelled on the diagram. One point has the coordinates (103, 0.325), and the second point has the coordinates (34, 0.188), where the coordinates take the following form: (W/S, T/W). The main priority is to maximize the wing loading and minimize the thrust-to-weight ratio. A high wing loading allows the wing to have a smaller reference area to generate the same amount of lift for the same-weight aircraft, which also results in reduced drag. A lower thrust ratio means that less thrust is required, which can reduce both operational and production costs as less power is required to operate the aircraft.

The first point on the left has a low T/W and a low W/S, while the point on the right has a larger T/W ratio with a higher W/S. Selection of one of these two optimal points becomes a matter of design choices, as there are pros and cons to both. The point that was ultimately selected is shown in orange on the diagram. This point was selected, as a higher wing loading would mean there is less surface area, meaning that the wing would need to generate more lift per surface area to maintain steady level flight during cruise. Increasing the lift requirement would increase the required angle of attack, which would increase the drag and approach stall faster. Due to difficulties finding a suitable engine designed in the current century with modern technology and the right parameters, an engine was selected with a thrust of 13 850 lb. Doubling this value totals 27 700 lb of thrust. Because the weight remained unchanged, the T/W ratio was automatically calculated.

Table 3-7: Selected T/W and W/S values from constraint diagram.

T/W	W/S
0.286	43

Two figures are presented below: Figure 3-11 shows the change in thrust with altitude, and Figure 3-12 shows how the best rate of climb and best climb airspeed change with altitude. The second figure was used to model the climb weight fractions in the weight analysis from Section 2. As the plane climbs in altitude, the best rate of climb gradually decreases, as the best climb airspeed which yields the best rate of climb increases to roughly 800 ft/s at cruise altitude. To determine the service ceiling, this point is assumed to be the point at which the best rate of climb falls below 100 ft/min, in order to include a marginal factor of safety, as opposed to setting the service ceiling to a climb rate of 0 ft/min. This point corresponds to approximately 70 000 ft, 5 000 above the cruise altitude. This should still allow the aircraft to cruise at 65 000 ft even on non-ideal days with large temperature deviations.

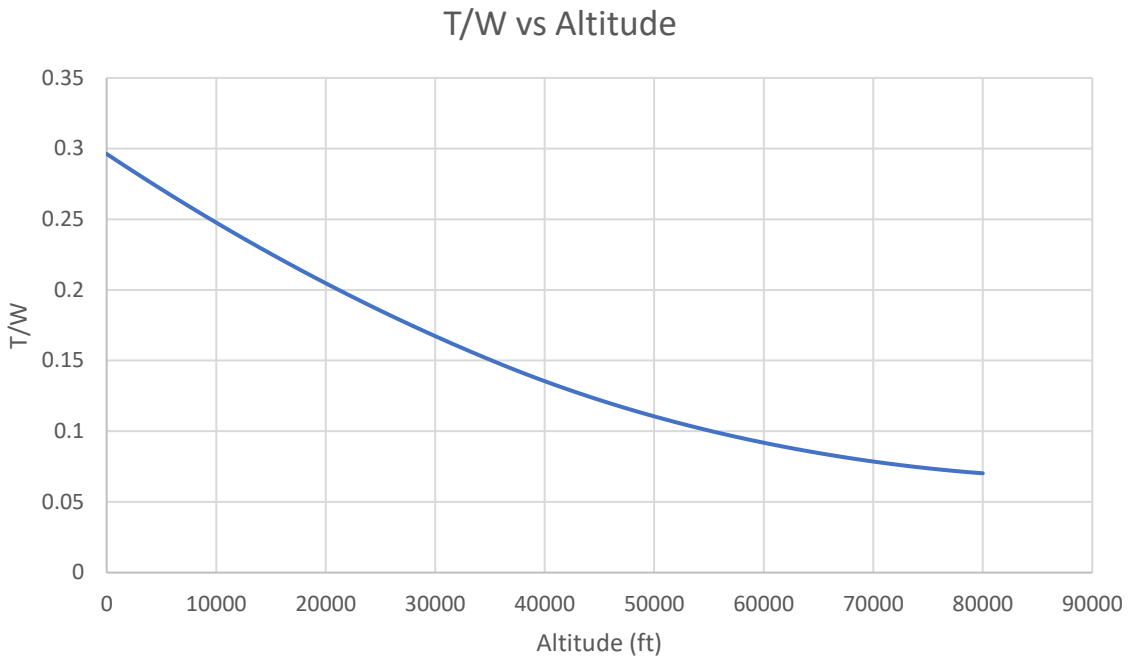

Figure 3-11: Thrust lapse with altitude.

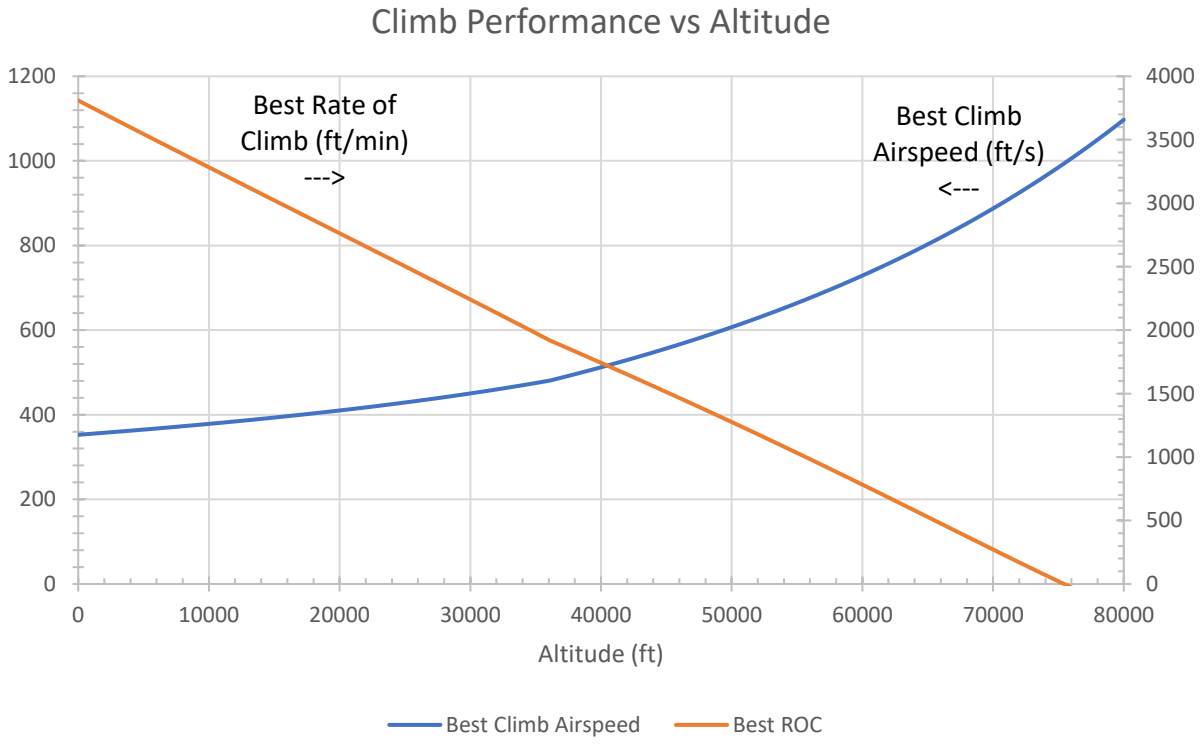

Figure 3-12: Variation of best ROC and best climb airspeed with altitude.

3.4 Sizing and Power

The power required by the aircraft is determined by the thrust-to-weight ratio of the constraint analysis. Based on the constraints, the ideal thrust-to-weight ratio is 0.286 and the wing load is 43 Since T/W = 0.286, W0=96804b, T=27686lbf, this makes the power requirement of each engine 13843 lbf. Based on this information, RR 611TAY was selected. The RR611TAY has an engine power rating of 13,850 lbf (sea level) and an SFC of 0.69. The RR611TAY is a low bypass ratio turbofan engine with a bypass ratio of 3.04. For high-altitude aircraft, jet engines are the best power plant, but they are less fuel efficient than turbojet engines. This affects range and requires more fuel, which increases weight. In this design, there is a trade-off for using a turbofan engine. The engine has less thrust at high altitudes but has better SFC, reducing fuel weight requirements at the expense of only a small percentage of thrust.

For the dimensions of this design, the optimal wing loading is 43 based on constraint analysis. At a weight of 96,000 pounds, the required wing is determined by W/S = 43, W=96,000 pounds, S= 2232.6 square feet. Design wingspan is 134.51 feet and AR is 8.04. These results are summarized in Table 3-8.

Table 3-8: Primary wing dimensions.

Parameter	Value
Wingspan	134.51 ft
Aspect Ratio	8.04
Taper Ratio	0.46
Sweep Angle	7.5°
Root Chord	22.97 ft
Tip Chord	10.5 ft
Wing Area	2250.73 ft^2

Therefore, the designed wing area is slightly larger than the required area, which meets the ideal wing loading requirement.

Specific wing and flaps dimensions can be found in the 3 views drawing and CAD model.

3.5 Performance

Using the wing loading and TWR selected from the constraint analysis, the some of the significant performance parameters are presented in Table 3-99-9.

Table 3-99: Performance parameters for SADIE-65.

Parameter	Symbol	Value	Units
Stall speed (clean wing)	V_S	86.4	KTAS
Stall speed (flaps T-O cond.)	V_{S1}	77.8	KTAS
Stall speed (flaps LDG cond.)	V_{S0}	71.3	KTAS
Ground roll @ SL	S_G	2800	ft
Total T-O distance @ SL	S_{TOT}	2 886	ft
Total T-O distance @ SL (ISA +61°F)	S_{TOT}	3 322	ft
Total T-O distance @ 2500 ft (ISA +57°F)	S_{TOT}	3 615	ft
Lift-off speed @ SL	V_{LOF}	85.5	knots
Best rate of climb	V_V	3 809	ft/min
Service ceiling	H	70 000	ft
Speed for best range	V_R	603	KTAS
Speed for best endurance	V_E	348	KTAS
Best glide speed	$V_{minsink}$	94.7	knots
Landing distance	S_{LDG}	4 442	ft

4 CONCEPTUAL STRUCTURE DESIGN AND FINALIZATION

4.1 V-n Diagram

The V-n diagram is a graphical representation illustrating the relationship between the load factor an aircraft can sustain and its speed. In this diagram, the speed of the aircraft is on the horizontal axis, while the vertical axis represents the loads applied to the aircraft structure. Loads are presented in terms of G forces experienced by the aircraft.

The four blue lines are the gust lines. For 14 CFR Part 25 the crustal gust speed is 56 fps, and the diving gust speed is 28 fps. The maximum and minimum G-forces that SADIE can withstand are 2.318 and –0.927 respectively, and the V_{s1} speed is 80 KEAS, V_c 200 KEAS and V_d 280 KEAS.

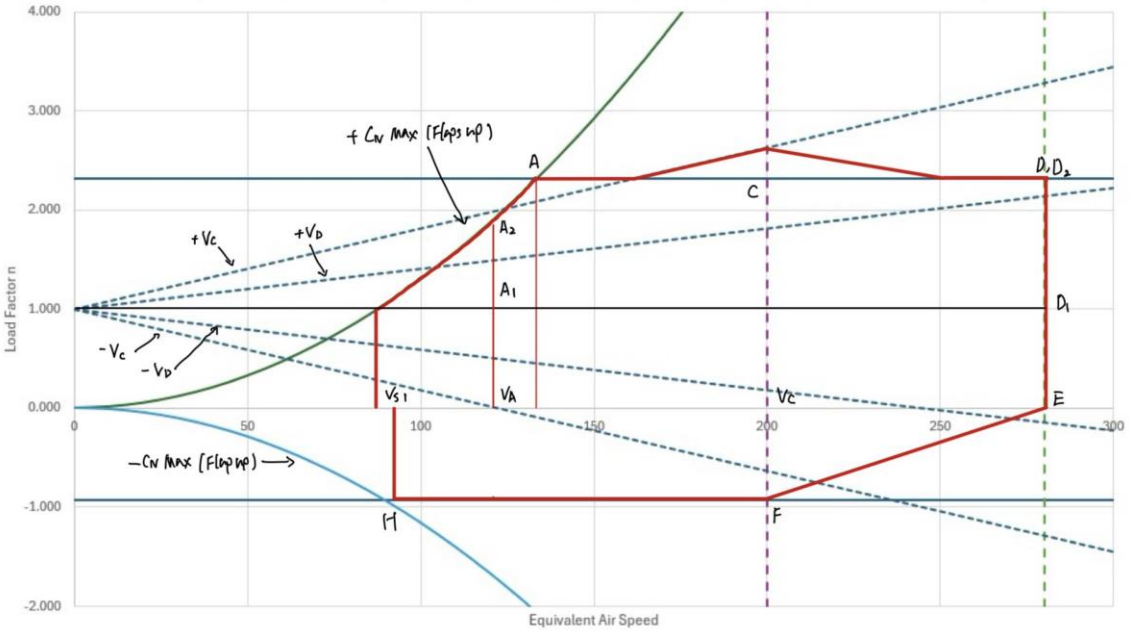

Figure 4-1: V-n diagram.

4.2 Concept Assessment

The design for SADIE-65 outlined in this document provides a good understanding of the aircraft which has been conceptualized. As stated in Section 1 when researching similar aircraft, there are currently not many which are capable of high-altitude flight and have large payload capacities simultaneously. Because of this lack of competition, acquisition of this concept would certainly be a good investment. Certain design choices were also led by aesthetics, which is reflected in the 3-view drawing and 3D rendering presented in Section 4.3. The aircraft uses conventional design components and features seen on many aircraft today and does not have a factor of uniqueness that makes it too undesirable by potential customers and pilots. It has a sense of familiarity, as it resembles many aircraft which already exist today. In terms of practicality, the aircraft has been designed and optimized to fulfill the mission at hand based on the requirements outlined in the RFP. With further design and optimization, the performance parameters can improve even further, while simultaneously decreasing both the production and operating costs.

In terms of uniqueness, SADIE-65 features a unique liquid payload-dispensing system not used in any aircraft today. This is also one of few aircraft capable of dispensing payload at high altitudes.

4.3 Final 3-View Drawing and CAD Model

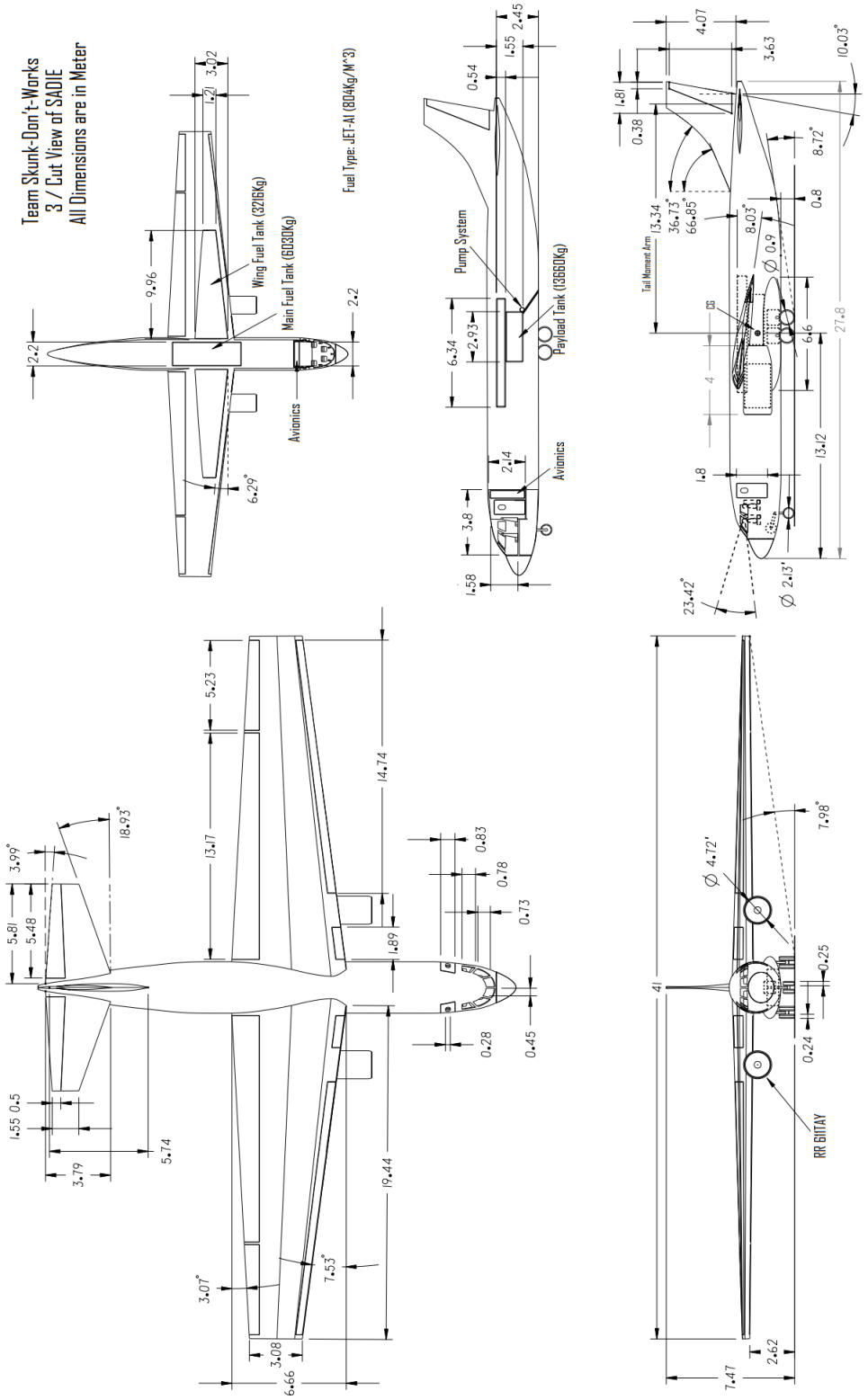

Figure 4-2: Final 3-view engineering drawing of SADIE-65.

Figure 4-3: 3D rendering of CATIA model of SADIE-65 cruising at altitude.

References

[1] M. Bradley, "Stratospheric Payload Delivery," AIAA, 2023.

[2] Aerospaceweb.org, "Aircraft Museum - B-52 Stratofortress," aerospaceweb.org, [Online]. Available: https://aerospaceweb.org/aircraft/bomber/b52/. [Accessed 15 Feb 2024].

[3] Aerospaceweb.org, "Aircraft Museum - SR-71 Blackbird," Aerospaceweb.org, [Online]. Available: https://aerospaceweb.org/aircraft/recon/sr71/. [Accessed 15 Feb 2024].

[4] Aerospaceweb.org, "Aircraft Museum - XB-70 Valkyrie," Aerospaceweb.org, [Online]. Available: https://aerospaceweb.org/aircraft/research/xb70/. [Accessed 15 Feb 2024].

[5] "U-2S/TU-2S," United States Air Force, September 2015. [Online]. Available: https://www.af.mil/About-Us/Fact-Sheets/Display/Article/104560/u-2stu-2s/. [Accessed 6 April 2024].

[6] M. d. Vreeze, "Walk around - Boeing B-52 Stratofortress," IPMS NEDERLAND, 11 May 2021. [Online]. Available: https://ipms.nl/walkarounds/walkaround-jets/walkaround-boeing-b52. [Accessed 7 April 2024].

[7] "U-2 Dragon Lady," aerospaceweb.org, [Online]. Available: https://aerospaceweb.org/aircraft/recon/u2/. [Accessed 7 April 2024].

[8] N. V. Nguyen, "The Simple Mission Profile of a Regional Jet Aircraft," 2011.

[9] S. Gudmundsson, "GENERAL AVIATION AIRCRAFT DESIGN," in *Aircraft Weight Analysis*, Elsevier, 2022, pp. 147-155.

[10] "Boeing 727," Wikipedia, 12 February 2024. [Online]. Available: https://en.wikipedia.org/wiki/Boeing_727. [Accessed 15 February 2024].

[11] "Hawker Siddeley Trident," Wikipedia, 2 February 2024. [Online]. Available: https://en.wikipedia.org/wiki/Hawker_Siddeley_Trident#Specifications. [Accessed 15 February 2024].

[12] "McDonnell Douglas DC-9," Wikipedia, 14 February 2024. [Online]. Available: https://en.wikipedia.org/wiki/McDonnell_Douglas_DC-9. [Accessed 15 February 2024].

[13] "Bombardier Global 7500," Wikipedia, 15 February 2024. [Online]. Available: https://en.wikipedia.org/wiki/Bombardier_Global_7500. [Accessed 15 February 2024].

[14] "Gulfstream G650/G700/G800," Wikipedia, 15 February 2024. [Online]. Available: https://en.wikipedia.org/wiki/Gulfstream_G650/G700/G800. [Accessed 15 February 2024].

[15] "Gulfstream V," Wikipedia, 24 December 2023. [Online]. Available: https://en.wikipedia.org/wiki/Gulfstream_V. [Accessed 15 February 2024].

[16] "Bombardier Global Express," Wikipedia, 14 February 2024. [Online]. Available: https://en.wikipedia.org/wiki/Bombardier_Global_Express. [Accessed 15 February 2024].

[17] "Dassault Falcon 7X," Wikipedia, 11 February 2024. [Online]. Available: https://en.wikipedia.org/wiki/Dassault_Falcon_7X. [Accessed 15 February 2024].

[18] "Boeing 737 Next Generation," Wikipedia, 15 February 2024. [Online]. Available: https://en.wikipedia.org/wiki/Boeing_737_Next_Generation#Specifications. [Accessed 15 February 2024].

[19] "Airbus A318," Wikipedia, 14 February 2024. [Online]. Available: https://en.wikipedia.org/wiki/Airbus_A318. [Accessed 15 February 2024].

[20] "Boeing B-47 Stratojet," Wikipedia, 3 February 2024. [Online]. Available: https://en.wikipedia.org/wiki/Boeing_B-47_Stratojet. [Accessed 15 February 2024].

[21] "Boeing B-52 Stratofortress," Wikipedia, 11 February 2024. [Online]. Available: https://en.wikipedia.org/wiki/Boeing_B-52_Stratofortress. [Accessed 15 February 2024].

[22] "Rockwell B-1 Lancer," Wikipedia, 13 February 2024. [Online]. Available: https://en.wikipedia.org/wiki/Rockwell_B-1_Lancer. [Accessed 15 February 2024].

Appendix

A. Sizing Analysis Sample Calculations

The following equations provide sample calculations for the final iteration of the preliminary sizing analysis. Assuming a gross weight of 96 804 lb, the empty weight will first be determined by fitting the logarithm of the gross weight to the trendline in Figure 2-2. The trendline has a slope of 0.0768 and an intercept of -0.3428. The empty weight fraction is calculated as follows:

$$\frac{W_e}{W_0} = AlnW_0 + B = (0.0768)\ln(96804) + (-0.3428) = 0.539$$

Next, the fuel weight fraction is determined. Using the data from Table 2-1, and referencing the nodes from Figure 2-1, the weight fractions for each mission segment can be determined using the following relationships.

$$\frac{W_1}{W_0} = 1 - (\Delta t_{taxi} r_{idle} + \Delta t_{max} r_{max}) SFC \qquad \text{(T-O)}$$

$$\frac{W_1}{W_0} = 1 - \big((0.33hr)(0.020) + (0.017hr)(0.286)\big)(0.737hr^{-1}) = 0.992 \text{ (T-O cont.)}$$

$$\frac{W_3}{W_2} = e^{-\frac{R * C_t}{V_{inf}\left(\frac{L}{D}\right)_R}} = e^{-\frac{(400nm)\left(0.690hr^{-1}\right)}{(400knots)(13.6)}} = 0.951 \qquad \text{(Cruise-No payload drop)}$$

$$\frac{W_4}{W_3} = 0.95 \qquad \text{(Descend)}$$

$$\frac{W_5}{W_4} = 0.99 \qquad \text{(Landing)}$$

Taking the product of all of the mission segment weight fractions calculated above, the total mission weight fraction can be determined and used to find the fuel weight fraction.

$$\frac{W_N}{W_0} = \prod_{i=1}^{N} \left(\frac{W_i}{W_{i-1}}\right) = (0.992)(0.938)(0.626)(0.95)(0.99) = 0.547 \qquad \text{(Total)}$$

$$\frac{W_f}{W_0} = 1 - \frac{W_N}{W_0} + \frac{W_p}{W_0} = 1 - 0.547 - \frac{30000}{96804} = 0.143 \quad \text{(FWF)}$$

With the empty and fuel weight fractions known, a new gross weight can be calculated using the following equation.

$$W_0 = \frac{W_c + W_p}{1 - \left(\frac{W_e}{W_0}\right) - \left(\frac{W_f}{W_0}\right)} = \frac{(800) + (30000)}{1 - (0.539) - (0.143)} = 96804$$

These calculations are then repeated using the design gross weight calculated above as the new guess. This process is iterated until the gross weights converge, and the guessed gross weight is equal to the calculated gross weight.

B. Tabulated Data from Sensitivity Study Plot (Figure 2-4)

Table B-1: Tabulated data for sensitivity analysis plot (Figure 2-4).

	Estimated Design Gross Weight (lb_f)				
% Change	**SFC**	**L/D**	**EWF**	**Payload**	**Range**
-65	86289	142588	43138	28088	87954
-60	87016	129628	44808	32503	88566
-55	87756	121478	46639	37074	89189
-50	88508	115841	48660	41796	89822
-45	89273	111697	50902	46666	90466
-40	90051	108517	53409	51680	91121
-35	90843	105996	56235	56837	91787
-30	91649	103948	59451	62133	92466
-25	92469	102250	63155	67569	93156
-20	93305	100819	67479	73142	93859
-15	94155	99596	72617	78853	94575
-10	95021	98540	78855	84700	95304
-5	95904	97617	86654	90684	96047
0	96804	96804	96804	96804	96804
5	97721	96083	110837	103061	97576
10	98657	95438	132347	109455	98363
15	99611	94859	173888	115987	99165
20	100584	94335	275273	122657	99984
25	101578	93859	-	129466	100819
30	102593	93425	-	136416	101672
35	103629	93027	-	143508	102542
40	104687	92662	-	150743	103431
45	105770	92324	-	158122	104339
50	106876	92012	-	165647	105268
55	108007	91722	-	173320	106217
60	109164	91453	-	181143	107187
65	110349	91201	-	189117	108180